Volume 2
Number 22
21 November 2021
Pages 7091–7492

Materials Advances

rsc.li/materials-advances

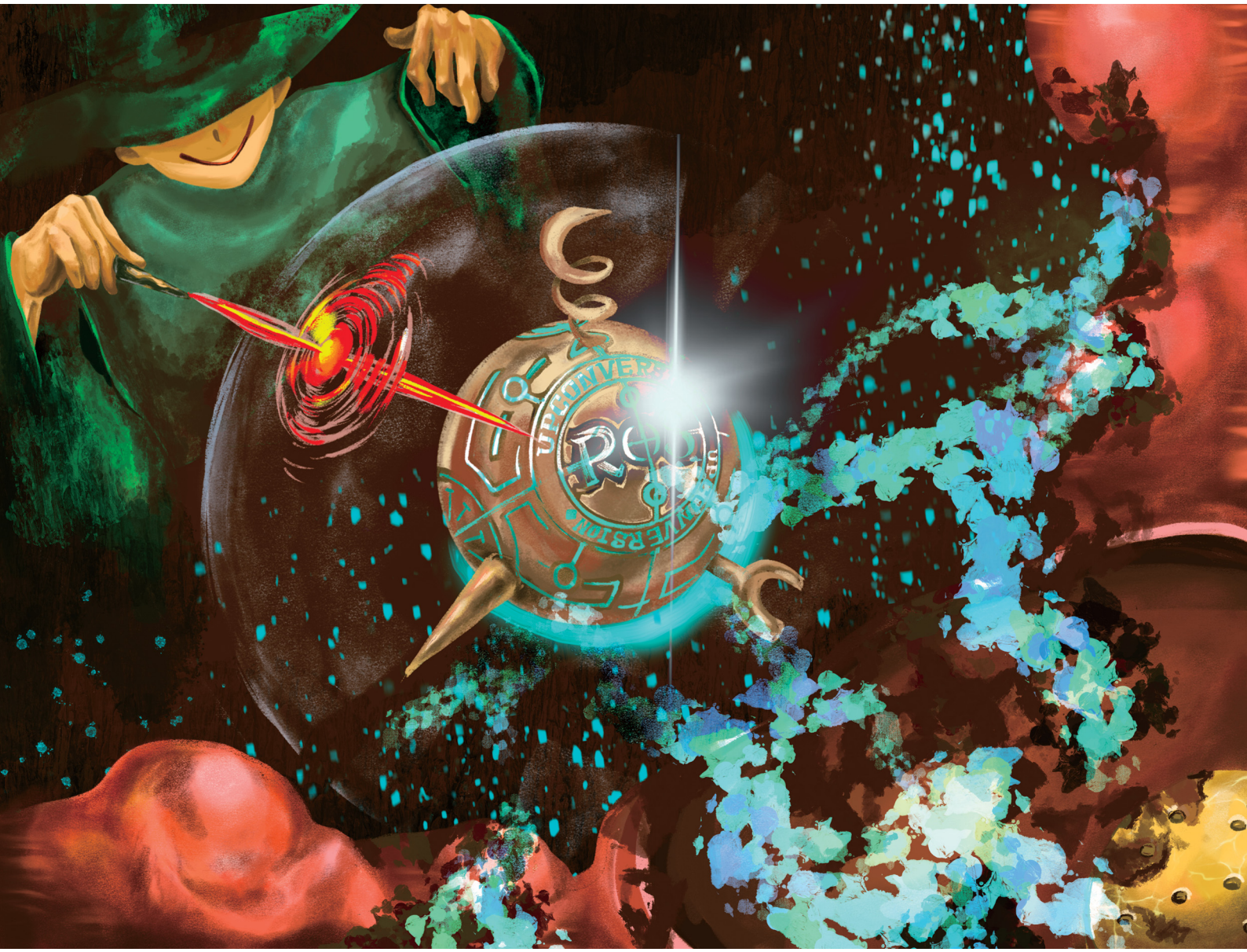

ISSN 2633-5409

ROYAL SOCIETY OF CHEMISTRY

REVIEW ARTICLE

Yu-Fen Huang, Hsin-Cheng Chiu *et al.*
Prospects of an engineered tumor-targeted nanotheranostic platform based on NIR-responsive upconversion nanoparticles

Materials Advances

ROYAL SOCIETY OF CHEMISTRY

REVIEW

View Article Online
View Journal | View Issue

Cite this: *Mater. Adv.*, 2021, 2, 7101

Prospects of an engineered tumor-targeted nanotheranostic platform based on NIR-responsive upconversion nanoparticles

Arjun Sabu,†[a] Jui-Yen Lin,†[b] Ruey-An Doong,[b] Yu-Fen Huang *[abc] and Hsin-Cheng Chiu *[a]

Theranostics, which affords both therapeutic and diagnostic functions within a single entity, has emerged as a cutting-edge technology for the development of personalized nanomedicine. Nanoparticles also offer the potential to unlock new avenues in cancer theranostics, attributed to their capacity for multifunctionality and multivalency. Lanthanide-doped upconversion nanoparticles (UCNPs) constitute a promising nano-scale platform notable for its unique ability to convert near-infrared (NIR) light into higher-energy luminescence. In addition to the large anti-Stokes shift, UCNPs also feature multiple sharp emission peaks varying from the ultraviolet (UV) to the NIR region, long luminescence lifespan, and high stability against photobleaching. By using NIR irradiation as an excition source, UCNPs enable deep-tissue bioimaging, controlled cargo release and subsequent therapeutic actions with high spatial and temporal resolution. On the other hand, to accomplish site-specific targetability to maximize theranostic outcomes, active targeting directed by specific tumor-homing ligands has been proven to be efficacious in improving tumor accumulation and reducing side effects. The choice of targeting ligands falls into several general classes including small molecules, peptides, proteins, antibodies, carbohydrates, or nucleic acid aptamers. Ligand-mediated targeting of functionalized UCNPs tailored with cancer-specific recognition moieties will lead to enhanced cellular uptake and permeability in tumor tissues, thus achieving effective theranostic treatments and long-term prognosis. In this perspective, we discuss the provision and prospects of specific ligand functionalized UCNPs for targeted delivery and theranostic application in various types of tumor therapies.

Received 28th June 2021,
Accepted 13th September 2021

DOI: 10.1039/d1ma00563d

rsc.li/materials-advances

[a] *Department of Biomedical Engineering and Environmental Sciences, National Tsing Hua University, Hsinchu, 30013, Taiwan. E-mail: hscchiu@mx.nthu.edu.tw*
[b] *Institute of Analytical and Environmental Sciences, National Tsing Hua University, Hsinchu, 30013, Taiwan. E-mail: yufen@mx.nthu.edu.tw*
[c] *School of Pharmacy, College of Pharmacy, Kaohsiung Medical University, Kaohsiung, 80708, Taiwan*
† The first and second authors contributed equally to this work.

Arjun Sabu

Mr Arjun Sabu received his master's degree from Cochin University of Science and Technology, India, in 2017. He is currently pursuing PhD in Biomedical Engineering and Environmental Science at National Tsing Hua University, Taiwan, under the supervision of Prof. Hsin-Cheng Chiu. His research interests include the synthesis and applications of multifunctional nanoparticle systems for drug delivery.

Jui-Yen Lin

Dr Jui-Yen Lin received his PhD in chemical engineering from National Cheng Kung University in 2020. His doctoral research focuses on the crystallization and adsorption processes in water purification. After obtaining his PhD, he started working with Prof. Doong at National Tsing Hua University as a postdoctoral research fellow, focusing on photoelectrocatalysis aided by photo upconversion. His present research interests include the synthesis of low-power upconversion materials and the photoelectrodes efficacious in water splitting and organic abatement.

1. Introduction

For decades, cancer has remained among the greatest threats to human health. In addition to surgery and radiotherapy, systemic therapy with chemotherapy is the most common treatment option. Unfortunately, chemotherapy often inflicts substantial damage on both cancer and noncancer cells, causing serious side effects.[1] Rapid drug elimination, nonspecific distribution, and the inadequate accumulation of therapeutics also result in a large number of drug administrations, which further exacerbates undesirable off-target effects. It is desirable to develop chemotherapeutics that can target cancer cells based on the specific changes in the molecular biology of tumor cells. Aside from the therapeutic interventions, imaging techniques including computed tomography (CT), magnetic resonance imaging (MRI), positron emission tomography (PET), and ultrasound (US) are currently accessible for the detection and diagnosis of cancer. Optical imaging, which provides high-resolution images covering a wide analytical scale from cells to organs, is also an invaluable tool for multimodality imaging.[2,3] The integration of diagnostic imaging and therapy, known as theranostics,[4] is a concept that is expected to promote accurate diagnosis, monitoring, and treatment at the anatomical and molecular levels. This approach is indisputably useful in the current era of precision medicine and has exerted a substantial impact on modern cancer medicine.

Recent advances in the use of nanoparticles (NPs) as a delivery platform have opened up a promising new avenue for precise and effective cancer management, mainly owing to their unique therapeutic controllability over the location, dosage and timing. Due to vascular abnormalities in rapidly proliferating cancer tissues, nanosized therapeutics preferentially accumulate at tumor sites through the enhanced permeability and retention effect.[5] Active targeting strategies dependent on complementary ligand–receptor binding have also been introduced to enhance both the intracellular delivery and the accumulation of drugs in tumors[6,7] to further improve the accuracy and efficacy in cancer nanotheranostics. This is achieved by functionalizing the surface of the nanocarrier with ligands that bind to receptors over-expressed on tumor cells. Subsequent initiation of receptor-mediated endocytosis can also promote the cellular uptake of nanoagents in cancer cells.[7,8] Thus, therapeutic payloads can be effectively delivered to the target site at an appropriate dosage, thereby reducing systemic toxicity. Folates and other small molecules, aptamers, proteins, peptides, antibodies, and hyaluronic acid (HA) are some representative targeting ligands used for this purpose.[9]

Nanovesicles respond "smartly" to exogenous and/or endogenous triggers, thereby enabling the precise control of on-demand therapy.[10,11] Endogenous stimuli such as pH, redox potentials, hypoxia, and enzymes are based on the physiological differences between cancer and healthy tissues. Among them, pH is a commonly used stimulus for controlled drug delivery, given that

Ruey-An Doong

Prof. Ruey-An Doong received his PhD degree from National Taiwan University, Taiwan. He is currently Chair Professor at National Tsing Hua University, and also serves as the Dean of Tsing Hua International College. He is internationally known for his research in environmental nanotechnology, energy materials, and biosensors and nanosensing devices. He has published over 200 papers with 10 000+ citations and h-index of 60. He is the recipient of the International Honorable Member Award from the American Academy of Environmental Engineers and Scientists and Fellow of the International Association of Advanced Materials (IAAM).

Yu-Fen Huang

Prof. Yu-Fen Huang received her PhD degree from National Taiwan University, Taiwan. She is currently a full professor at National Tsing Hua University, and also serves as the Chairman of the Inter-disciplinary Program of Nuclear Science at National Tsing Hua University. Her research includes the development and design of multifunctional nanomaterials for targeted therapy and controlled drug release. She has published more than 100 scientific papers in the fields of biosensing, functional nanomaterials and cancer therapeutics.

Hsin-Cheng Chiu

Prof. Hsin-Cheng Chiu received his PhD degree from the Department of Pharmaceutics and Pharmaceutical Chemistry, University of Utah. He is now a full professor at National Tsing Hua University. His research includes the design of targetable therapy delivery systems and triggered drug release devices and the synthesis of new biomaterials for drug delivery applications. He is the Fellow of Biomaterials Science and Engineering (FBSE) and currently serving as the President of Taiwan Biomaterials and Controlled Release Society. He has published more than 100 scientific papers in the biomaterials and drug delivery field.

the tumor microenvironment (TME) is more acidic (pH 6.5–6.9) than the normal tissue environments (pH 7.2–7.4).[12] The pH also gradually decreases after entering the cells through endocytosis, decreasing to a value as low as pH 5.0–6.0 in endosomes and 4.0–5.0 in lysosomes.[13] Accordingly, engineered NPs with ionizable groups or blocks or acid-labile bonds can trigger selective drug release at the target site upon exposure to variations in pH.[10,11,14] External forces including light, magnetic field, electric field, and US are also appropriate stimuli to control the delivery and activation of therapy.[10,11] Light is especially attractive as a stimulus due to its non-invasiveness, high spatiotemporal resolution, and ease of remote control.[15–17] For instance, photodynamic therapy (PDT) uses light as an energy source to activate photosensitizers (PSs) to produce reactive oxygen species (ROS) that can destroy surrounding cancer cells.[18] Photothermal therapy (PTT) uses light to excite ablation agents (*e.g.*, organic dyes or plasmonic NPs) to increase the local temperature and damage malignant tissues.[19] However, most of the light interventions involving irradiation are in the ultraviolet (UV) and visible spectral ranges (wavelengths < 650 nm). Problems include potential phototoxicity, limited tissue penetration, and high autofluorescence in biological species.[20] The recent development of nanotheranostics based on the near-infrared (NIR) spectral window (650–950 nm) has garnered considerable research interest aimed at maximizing its performance.[19,21,22] Plasmonic NPs, transition metal chalcogenides, and carbon derivatives are representative examples of NIR harvesting transducers, which have been widely adopted in PTT or PDT.

Lanthanide-doped upconversion nanoparticles (UCNPs) constitute a novel class of luminescent nanomaterials notable for their unique efficiency in converting NIR light into higher-energy UV and visible light.[23] Upon NIR irradiation, UCNPs with appropriately doped ions exhibit upconversion (UC) photoluminescence with broad-spectrum tunability. With the added benefits of large anti-Stokes shifts, sharp emission bandwidths, and long excited-state lifetimes, UCNPs can achieve orthogonal emissions, spectral/lifetime multiplexing, and multimodal imaging with improved signal-to-noise ratios and high spatial resolution.[24–27] UCNPs also possess attractive features including low toxicity, favorable biocompatibility, and excellent photostability. When surface engineered with targeting ligands, drugs, or other therapeutic agents, UCNPs have been identified as a promising multifunctional tool associated with desirable diagnostic and therapeutic outcomes for theranostic therapy targeting deep tumor tissues.[28–32]

In this review, we present the luminescence characteristics of UCNPs and their rational design for cancer diagnosis and treatment (Fig. 1). The synthesis and surface modification processes of UCNPs are also illustrated. Notably, recent advances in the development of UCNPs in targeted cancer theranostics and tumor-specific drug delivery are described. Approaches for fine-tuning UCNPs with high upconversion (UC) efficiency, tunable output wavelengths, and magnetic or radioactive properties are discussed to serve as a reference for multimodal imaging and theranostic applications. Furthermore, sophisticated strategies allowing switchable, hierarchical, or dual targeting, providing new insights into precision nanomedicine development, are discussed. Finally, we present the conclusion and future challenges in UNCP-based cancer therapy.

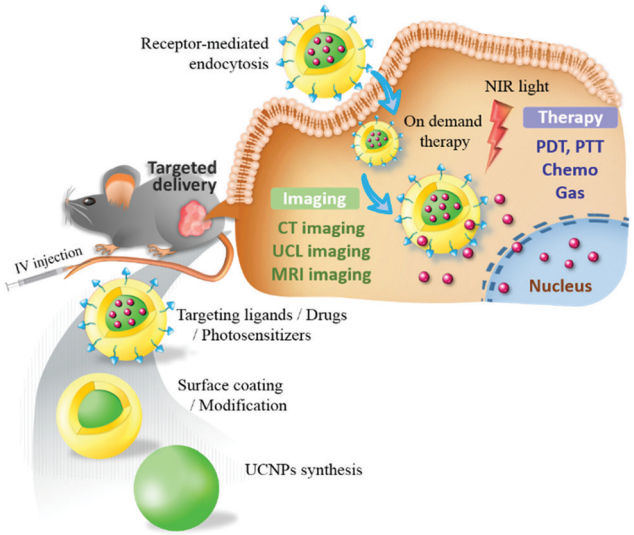

Fig. 1 Targeted UCNPs as an engineered NIR-responsive theranostic nanoplatform for tumor-targeted imaging and therapy.

2. Rational design of UCNPs as a potential nanotheranostic platform

UCNPs are lanthanide-doped NPs that can upconvert two or more absorbed photons with lower energy (generally NIR light) into a high-energy photon (*e.g.*, from NIR, visible, or UV light). Unlike conventional molecular fluorophores or quantum dots that require the simultaneous absorption of two or more photons, UCNPs provide greater cross-sectional absorption in NIR,[23,33] a sequential absorption process, and multiple long-life intermediate states, thereby leading to enhanced UC efficiency of up to several orders of magnitude. They also allow UC to be produced using low-cost continuous-wave diode lasers without the need for ultrashort pulsed lasers.[34] However, factors such as lanthanide ions, host lattices, and core–shell architectures play a decisive role in leveraging the energy transfer process and the luminescence performance. The surface coating and functionalization of UCNPs are also crucial in determining their biological outcomes. In this section, approaches that can lead to the rational design of UCNPs for effective theranostic applications are explored.

2.1 Luminescence mechanism and properties of UCNPs

The luminescence of UCNPs derives from the intra-4f electron transitions of lanthanide ions that are doped within an appropriate host crystal. Because the 4f electron orbitals of lanthanides are well shielded by the outer 5s and 5p electrons, these intra-4f electron transitions feature long lifetimes of approximately several milliseconds, enabling the electron to be excited multiple times prior to radiative relaxation and resulting in upconversion

luminescence (UCL).[35] The host crystal has a substantial effect on the UC efficiency of UCNPs. To facilitate the against-nature intra-4f electron transitions, lanthanides must be embedded in the host crystal featuring low crystal field symmetry to modify the 4f electron wavefunctions of lanthanides such that parity-forbidden electron transitions are partially allowed.[36] The host crystals of UCNPs should also have low lattice phonon energy to minimize nonradiative energy loss.[35] Among the various candidates for UCNP host, transition metal halides such as $NaYF_4$, $LiYF_4$, and $NaGdF_4$ are preferred for their excellent promotion of UC efficiency and their physicochemical stability.[37]

The selection of lanthanides to be doped in UCNPs is another key factor in achieving efficient energy transfer for UC. The lanthanide atoms in UCNPs are trivalent and feature ladder-like 4f energy levels that determine the wavelength of the photons that can be absorbed and emitted.[38] Modern designs of UCNPs include the use of two varieties of lanthanides, sensitizers, and activators as dopants to maximize UC efficiency. The sensitizer is intended to absorb the incident photons, and its excited energy is transferred to the activator, which emits an upconverted photon after multiple excitations. Thus, the sensitizer determines the wavelength at which the UCNPs are excited, and the activator controls the wavelength of the upconverted photons. Sensitizers commonly used in UCNPs are Yb^{3+} and Nd^{3+}, both of which can be excited in the optical transmission window of tissues (700–1000 nm; Fig. 2). Yb^{3+} features a single excited-state energy level of $^2F_{7/2} \rightarrow {}^2F_{5/2}$ that can be excited by the photons from 920 to 1050 nm (maximum at 980 nm).[39] However, the pump wavelength of 980 nm resides in the absorption region of water and therefore leads to localized overheating of the tissue, which in turn limits the efficacy of *in vivo* deep-tissue biomedical applications.[39] Therefore, Nd^{3+}-sensitized UCNPs were developed so that the UC can be excited by an 808-nm laser ($^4I_{9/2} \rightarrow {}^4F_{5/2}$) to both minimize the overheating effect and exploit the large absorption cross-section of Nd^{3+} (1.2×10^{-19} cm^2, approximately 10-fold that of Yb^{3+}).[39] Because Nd^{3+} has multiple excitation states that may lead to excessive cross-relaxation, UCNPs cosensitized by Nd^{3+} and Yb^{3+} were developed to achieve higher UC efficiency, in which the excitation energy of Nd^{3+} is first indirectly transferred to the activator through Yb^{3+}.[40,41]

Common activators of UCNPs for therapeutic and diagnostic purposes include Er^{3+}, Ho^{3+}, and Tm^{3+}; the first two feature green- and red-light emission, whereas the third features NIR and blue light emission.[38] The selection of the activator depends on the function of the theranostics. For instance, the emission of the activator must match the excitation wavelength of the PS in PDT for cytotoxic ROS to be produced.[42] Likewise, the spectral overlap of the emission of the activator and the absorption of the photothermal (PT) agent is required whether PTT is used alone or in combination with PDT.[43] For photostimulated drug release, the activator should emit light at the required wavelength to photolyze the photoresponsive molecules and release the therapeutic agents.[44] UCNPs intended for deep-tissue imaging require activator emission within the transparency window.[33]

The emission of UCNPs governed by the activator can also be manipulated *via* the energy transfer pathway. Mechanisms of energy transfer between lanthanides, which have been extensively investigated, include excited-state absorption, energy transfer upconversion, cooperative sensitization upconversion, cross-relaxation, and photon avalanches.[28,45]

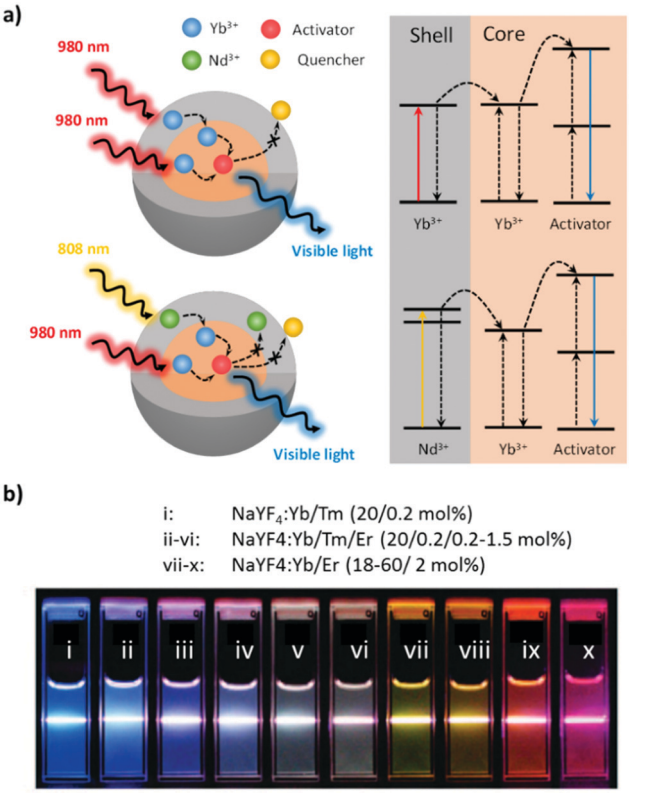

Fig. 2 (a) Mechanistic diagram of Yb-sensitized and Nd/Yb-cosensitized core–shell UCNPs. (b) Effects of activators on the emission of UCNPs excited at 980 nm. Reproduced from ref. 46 with permission from the American Chemical Society.

2.2 Synthesis and design of UCNPs for enhanced UCL

As mentioned, UCNPs have two components – host crystals and doped lanthanides – as sensitizers and activators, respectively. UCNPs for therapeutic delivery should have a size of 30–80 nm with a narrow distribution and high water dispersibility. Brightness maximization requires minimal crystal defects, as well as the proper concentration and even distribution of lanthanide dopants in the host crystal. To achieve this goal, numerous simple processes have been developed for UCNP synthesis, including thermolysis, hydrothermal processing, coprecipitation, and the sol–gel process.[45] Thermolysis and hydrothermal processing are preferred because the supersaturation can be easily controlled to facilitate the growth of high-quality crystals.[28] Thermolysis decomposes the organic precursor of lanthanide (usually metallic trifluoroacetate salts) in a solvent at elevated temperature and ambient pressure. To suppress the aggregation and overgrowth of UCNPs, a surfactant such as oleic acid, oleylamine, or trioctylphosphine is introduced as a capping agent. The size, shape, and phase of UCNPs can be tuned by the types and concentrations of the metal precursor and capping

agent, solvent, reaction temperature, and time. Although thermolysis can produce high-quality UCNPs with strong UCL and low polydispersity at ambient pressure, it requires high temperatures and expensive precursors that yield toxic fluorinated or oxyfluorinated organic byproducts.[38] In hydrothermal processing, UCNPs are synthesized at lower temperatures but under higher pressures. With inorganic lanthanide precursors (chloride, nitrate, or sulfate salts), UCNPs are obtained through nucleation and crystal growth near the critical point of the solvent.[28] Likewise, surfactants are the keys to ligating the precursors, controlling crystal growth, and preventing aggregation in UCNPs. Oleic acid and oleylamine are commonly exploited for such purposes, which leads to the capping of UCNPs with a hydrophobic surface group.[47] Alternatively, hydrophilic surfactants such as polyethylenimine (PEI) can be used as capping agents to produce biocompatible UCNPs without further surface modification.[48]

The UCL of UCNPs is determined by the absorption ability of the excitation light, the efficacy of the energy transfer, and the extent of defect and surface quenching. Numerous advanced designs have been proposed to enhance the UC efficiency of UCNPs, including those involving the doping of nonluminescent cations, the incorporation of dyes, plasmonic materials, and core–shell architectures.[28] To mitigate the problem of the low extinction coefficient of lanthanides, organic dyes are employed as external antennae for collecting the excitation light.[49] Organic dyes have broadband absorption and large absorption cross-sections, and the absorbed energy can be transferred to the UCNP sensitizer which greatly enhances the emission.[50] In addition, organic dyes can serve as PT agents to induce the PTT effect at the same time. Moreover, the presence of plasmonic metallic NPs has been reported to either enhance or quench the UCL of UCNPs, depending on the size and the surface plasmon resonance (SPR) wavelength of the plasmonic materials, as well as their distance to the UCNPs. If the SPR wavelength matches the excitation of the UCNPs, more energy can be harvested by the sensitizer, leading to enhanced UCL.[51] When the SPR wavelength overlaps with the UCNP emission, two energy transfer routes may be involved: nonradiative resonance energy transfer (RET), which quenches the UCL, and the Purcell effect, which enhances the radiative decay rate of the activator.[52] As the Förster mechanism is the main nonradiative RET route, the distance between the emitter and the plasmonic nanoparticle dictates the decay rate. On the other hand, the Purcell effect can increase the spontaneous emission rates of the emitter by elevating the local density of optical states under the electromagnetic field amplified by the plasmonic NPs. Purcell enhancement is highly dependent on the size and shape of the plasmonic NPs. Much effort has been dedicated to minimizing UCL quenching and improving the brightness of UCNPs by incorporating plasmonic NPs of different sizes.[52] The combination of plasmonic nanomaterials and UCNP provides an effective means to design high-sensitivity photoluminescence biosensing platforms.

Due to the high surface-to-volume ratio of nanosized UCNPs, surface defects, which greatly quench the upconverted emission, are abundant. Core–shell architectures were developed to prevent the excessive transfer of nonradiative energy in the vicinity of the UCNP core. These architectures not only effectively eliminate surface quenching but also boost energy transfer.[28] Based on the host matrix composition of the core and the shell, as well as on the introduction of lanthanide dopants (generally the sensitizer) to the shell layer, the shell structures can be active; they can also be homogeneously or heterogeneously inert. Core–shell architectures can be synthesized through seed-mediated growth, Ostwald ripening, and layer-by-layer assembly.[53] In general, the host crystal of the shell should have minimal lattice mismatches with the lattice of the cores, thus favoring epitaxial growth. If the shells are active (*i.e.*, doped with lanthanides), not only can the light-harvesting ability of UCNP be improved, but the energy migration path can also be adjusted to prevent the excessive cross-relaxation that quenches luminescence.[35]

2.3 Surface modification and functionalization of UCNPs

In targeted theranostics, UCNPs must be surface-hydrophilic, dispersible, biocompatible, and grafted with multiple functional groups.[37] To achieve these goals, the surface properties must be adjusted to be hydrophilic, because pristine UCNPs are capped by hydrophobic ligands such as oleic acid, oleylamine, or trioctylphosphine. Targeting ligands should also be properly engineered on the surface of UCNPs for efficient delivery. In addition, the use of light-responsive moieties to connect the therapeutic agents with UCNPs can maximize the effectiveness of treatment through on-demand cargo release. According to functionalization and linking strategies, the hydrophobic ligands on UCNPs can be altered using ligand removal, exchange, or oxidation for subsequent connection with hard materials, soft polymers, or biomolecules.[28]

Among the hard materials integrated with UCNPs, silica is the one most often applied given its biocompatibility, hydrophilicity, optical transparency, and favorable conjunction with targeting ligands. Generally, UNCP core–shell composites with silica encapsulation can be prepared through the sol–gel process. For UCNPs with hydrophilic surfaces, the Stöber method enables the growth of silica through hydrolysis and the condensation of alkyl silicate in the presence of ammonia as a catalyst. Through the reverse micelle method, silica is coated on hydrophobic UCNPs by creating surfactant-stabilized nanoreactors (*i.e.*, through microemulsion).[54] The advantage of silica-encapsulated UCNPs is that the surface functional groups can easily be tailored to have the end groups $-NH_2$, –COOH, or –SH through silanization, allowing further conjugation with biomolecules for targeted theranostics. Furthermore, the large surface area and pore volume of mesoporous silica are conducive to high drug loading, greatly improving the efficacy of PDT, PTT, and chemotherapy.[54] Metal–organic frameworks (MOFs) are an emerging class of porous materials that can be incorporated with UCNPs through direct crystal growth. To ensure the growth of MOFs on the surface of UCNPs, poly(vinylpyrrolidone) (PVP) is used. Being a well-known stabilizer, PVP can strongly coordinate with metal ions and thus bridge the gap between UCNPs and MOFs.[55] In addition to its use in drug loading, various MOFs have been developed for controlled drug release under external stimuli such as pH, light,

redox potentials, and temperatures.[56] UNCP modification with soft polymers or macromolecules is simple and essential for long-term dispersion stability. The reported polymers include poly(ethylene glycol) (PEG), PVP, poly(acrylic acid), PEI, and poly(maleic anhydride-*alt*-1-octadecene).[57] In general, hydrophobic interactions allow the coverage of UCNPs with amphiphilic polymers, although some are designed to graft polymers after silica encapsulation. As stimuli-responsive polymers have seen great advances in drug delivery and triggered release,[11] block or graft copolymers with functionalized designs have been used to endow UCNP-based nanotheranostics with desirable properties.

The loading of targeting ligands and therapeutic agents such as PSs and anticancer drugs on UCNP-based nanotherapeutics can be achieved through covalent bonding, electrostatic attraction, or hydrophobic interaction.[55] Covalent bonds provide strong linkages. Carbodiimide coupling agents, namely, EDC and NHS, are a classic example of covalent bonding in which an amine group is tightly joined with a carboxylic group. Because numerous targeting ligands feature amine groups, EDC and NHS can be widely adopted for ligand functionalization, wherein the surface of UCNPs is grafted with a sufficient number of carboxylic groups.[58] By contrast, electrostatic and hydrophobic interactions involve noncovalent bonds that play a pivotal role in supramolecular self-assembly. The hydrophobic interaction is the major process to encapsulate lipophilic PSs and chemotherapeutics in the polymer or mesoporous shells of UCNPs.[37] Layer-by-layer assembly, driven mainly by electrostatic interactions, can effectively deposit the next layer of oppositely charged polymers or therapeutic agents.[28] Meanwhile, the (de)protonation that causes the charge change from the surface or associated cargo also determines the pH-responsive controlled release behavior upon entry into the acidic TME or intracellular compartments. More representative examples are presented in the next section.

3. Biological ligand-mediated targeted theranostics based on multifunctional UCNPs

Numerous biological ligands, including small molecules, nucleic acid aptamers, proteins, peptides, and polysaccharides, have been identified and employed for the active targeting of NPs in diseased tissues, commonly tumor tissues (Table 1). Cell membrane–camouflaged NPs have also emerged as a new class of biomimetic NPs with attractive biological properties and functions such as immunosuppressive capability, long circulation time, and target recognition. The targeting ligands can both bind to specific receptors on the surface of the targeted cells to increase cellular uptake and target subcellular organelles to enhance the therapeutic effect, thereby maximizing theranostic outcomes and minimizing adverse effects. In this section, different types of biological ligands and their current applications in UCNP-based theranostics are reviewed, with the focus primarily on *in vivo* studies (Table 2).

3.1 Folates or small molecules

Folate or folic acid (FA) is a low-molecular-weight (M_w 441.4 Da) water-soluble vitamin and an indispensable nutrient for various cellular metabolic processes. Folate receptors (FRα, FRβ, and FRγ) are cysteine-rich cell-surface glycoproteins that can bind to folate with high affinity ($K_d < 1$ nM) in order to mediate folate uptake through endocytosis.[59] The increased folate requirement in rapidly proliferating cells, such as cancer cells,

Table 1 Ligands for the active targeting of UCNP-based theranostics

Type	Ligand (examples)	Surface receptors	Advantages	Disadvantages
Small molecules	Folate, glycyrrhetinic acid (GA)	Folic acid receptor (FR), GA receptor	• Small size ($M_w < 900$ Da) • Low cost • Ease to synthesize and modify	• Low specificity
Aptamers	AS-1411, sgc8	Nucleolin, tyrosine kinase 7	• Moderate size ($M_w \sim 5$ to 15 kDa) • Non-immunogenicity • Ease to synthesize and modify • Mainly from *in vitro* selections	• Rapid degradation by nuclease
Proteins	Antibodies, transferrin	Specific antigens, transferrin receptor (TfR)	• High specificity and affinity • Produced *in vitro* or *in vivo* • Long *in vivo* half-life	• Large size • High cost • Low stability • High immunogenicity • Limited permeability
Peptides	RGD	Integrin $\alpha v\beta 3$	• Moderate size (typically < 30 amino acids) • Non-immunogenicity • Ease to synthesize and modify • *In vitro* evolution	• Susceptible to peptidase
Polysaccharides	Hyaluronic acid (HA)	CD44	• Biocompatible and biodegradable • Non-immunogenicity • Ease to modify • Potential carrier in drug delivery	• Off-target effect
Cell membranes	Cancer cell membrane	Tumor-specific targeting	• Long circulation time • Immune escape • Homotypic targeting	• Tedious preparation methods • Low production yield • Batch-to-batch variation • Difficult to store • Potential safety concern

Table 2 Examples of multifunctional UCNPs for targeted theranostics

Type of ligand	Nanoagent	Type of UCNPs	Excitation wavelength (nm)	Therapeutic cargo	Type of carcinoma	Theranostic action	Ref.
Folic acid (FA)	FA-UCNPs	$NaYF_4$:Yb,Tm,Fe@$NaGdF_4$	980		Cervical cancer (HeLa)	UCL/MR/X-ray imaging	63
	FA-PEG-UCNs	$NaYF_4$:Yb,Er	980	MC540; ZnPc	Mouse melanoma (B16-F0)	PDT	65
	FPUMZ	$NaYF_4$:Yb/Er/Nd@$NaYF_4$:Nd	808	MC540; ZnPc	Cervical cancer (HeLa); mouse liver cancer (H22)	PDT	67
	GGBDFs	GdOF:Yb/Er	980	GNDs; DOX	Mouse cervical cancer (U14)	UCL/MR/CT imaging; chemo-PTT	68
	CUSCs-PEG-FA	$NaGdF_4$:Yb,Tm@ $NaGdF_4$:Nd,Yb	808	g-C_3N_4; CuS	Mouse cervical cancer (U14)	UCL/MR/CT imaging; PDT/PTT	70
	Bio-LTA-UCNPs	Er/Yb-LTA	980	DOX; PpIX	Mouse melanoma (B16-F0)	SDT/PTT/PDT/Chemotherapy	71
	Caged UNCPs	$NaYF_4$:Yb,Tm	980	DOX	Cervical cancer (HeLa)	UCL imaging; chemotherapy	73
Glycyrrhetinic acid (GA)	GA-CSS UCNPs	Li(Gd,Y)F_4:Yb,Er/LiYF_4:Nd,Yb/LiGdF_4	800		Liver cancer (HepG2)	UCL imaging	78
Aptamer	PT-UN	$NaGdF_4$:Yb,Er@ $NaYF_4$@$NaYF_4$: Yb,Tm@$NaYbF_4$:Nd@$NaYF_4$	808; 980	RB	Mouse breast cancer (4T1)	UCL imaging; PDT	95
	UCNPs@PDL@dsDNA/ DOX	$NaYF_4$@$NaYF_4$:Yb,Tm/Ho@$NaYF_4$	980	DOX	Non-small cell lung cancer (A549)	Chemotherapy	96
Protein	UCNP@PFSBT@Tf@Tc	$NaYF_4$:Yb/Tm	980	PFSBT; Tc	Mouse liver cancer (H22)	PDT	101
Antibody	CEA-UCNPs	$NaYF_4$:Yb/Er@$NaGdF_4$	980		Colon cancer (LoVo)	*In vivo* MRI; *ex vivo* UCL imaging	105
	UPG-CD326	$NaYF_4$:Yb,Er@$NaGdF_4$	980		Pancreatic cancer (BxPc-3)	UCL/MR imaging	110
	Anti-EpCAM-UPGs-MX	$NaYF_4$:Yb,Er@$NaGdF_4$	980	Mitoxantrone (MX)	Liver cancer (BEL-7404)	UCL/MR imaging; chemo-PDT	111
Peptide	UCNP-RGD	$NaYF_4$: Yb,Er,Tm	980		Glioblastoma (U87MG); breast cancer (MCF-7)	UCL imaging	114
	UCNP@TTD-cRGD	$NaYF_4$:Yb,Er	980	TTD	Breast cancer (MDA-MB-231)	PDT	115
	rUCNPs@HSA(Ce6-Mn)-RGD	$NaScF_4$:Yb,Er@CaF_2	980	Ce6-Mn	Glioma (U87)	MR imaging; PDT	116
	UCNP-ICG-TOS-RGD	$CsLu_2F_7$:Yb,Er,Tm	808; 980	α-TOS; ICG	Glioblastoma (U87MG)	UCL/CT imaging; chemo-PTT	117
	UCNP-Gd-RGD	$NaYF_4$:Yb,Er	980		Glioblastoma (U87MG)	UCL/MR imaging	120
	ANG-IMNPs	$NaYF_4$:Yb,Er,Mn	808; 980	IR-780; mTHPC	Murine astrocytoma (ALTS1C1)	PDT/PTT	122
	UCNP-RB/PNBMA-PEG-KE108	NaYF4:Yb/Er/Tm	980	RB; AB3	Neuroendocrine tumor (TT)	UCL imaging; chemo-PDT	126
	UCNP-P_n	$NaGdF_4$:Yb,Er@$NaGdF_4$	980		EBV(+)-nasopharyngeal carcinoma (C666); cervical cancer (HeLa)	UCL imaging	125
Hyaluronic acid (HA)	mUCNPs@DOX/CuS/ HA	$NaYF_4$:Yb, Er@$NaGdF_4$	980	CuS; DOX	Mouse sarcoma cancer (S180)	UCL/MR/PAT imaging; chemo-PTT	131
	UCTA NCs	$NaYF_4$:Yb/Tm@$NaYF_4$:Yb@$NaNdF_4$: Yb@$NaYF_4$	808	TiO_2; Hypocrellin A	Cervical cancer (HeLa)	PDT	132
	UCNP-IONP/PB-PEG-HA	$NaYF_4$:Yb,Er	808; 980	PBNPs	Mouse sarcoma cancer (S180)	UCL/MR imaging; PTT	133
	UCNPs-PEIRB-PEISeSe/ siRNA-R8-HA (UCNO)	$NaYF_4$:Er,Yb@$NaYF_4$:Yb,Nd	808	RB; siRNA	Liver cancer (HepG2)	Gene therapy	134
Cell membrane	FA-RBC-UCNPs	$NaYF_4$:Er,Yb	980		Breast cancer (MCF-7)	UCL imaging	140
	RBC micro-vehicles (RBCmv)	$NaGdF_4$:Yb, Tm@$NaGdF_4$	980	Hemoglobin; PTX	Mouse ovarian tumor	O_2 therapy; chemotherapy	141
	CC-UCNPs	$NaYF_4$:Er,Yb	980		Breast cancer (MDA-MB-435)	UCL imaging	142

yields higher FRα levels compared with that in normal cells. Thus, FA receptors are overexpressed in human carcinomas, including breast, ovarian, lung, brain, and colon cancers, but are only minimally distributed in normal tissues.[59] FA is among the most commonly used targeting molecules for the treatment and diagnosis of cancers.[60] Stability, inexpensiveness, and nonimmunogenicity (compared with that of monoclonal antibodies) are among its advantages. Companies such as Endocyte Inc. are developing products at different phases of clinical trials involving the loading of various drugs in FA-modified nanocarriers for the targeting of pathologies such as cancer, rheumatoid arthritis, and kidney disease.[61]

As mentioned, UCNPs are promising biolabels useful for biomedical imaging and cell tracking. For example, three FA-functionalized UCNPs (UCNC-Er-FA, UCNC-Tm-FA, and UCNC-Er,Tm-FA) were designed for *in vitro* UCL imaging of HeLa cells under the excitation of a 980-nm laser.[62] By doping $NaYbF_4$ with three types of rare-earth ions (Yb^{3+}/Er^{3+}/Tm^{3+}), a four-color (blue, green, red, and NIR) UCL output can be produced. Moreover, the NIR-to-NIR UCL efficiency of $NaYF_4$:Yb,Tm NPs was shown to be significantly enhanced (by approximately 20-fold) through tridoping with nonluminescent Fe^{3+} cations.[63] When the inert $NaGdF_4$ shell is incorporated into the core NPs of cit-Y:Yb,Tm,Fe, a further increase in UCL intensity can be observed (Fig. 3a). Furthermore, because Gd^{3+} ions exhibit strong paramagnetism and high X-ray attenuation ability, their doping also endows core–shell UCNPs with enhanced contrast in MRI and X-ray imaging. The introduction of FA can successfully accomplish tumor-targeted UCL/MR/X-ray trimodal imaging *in vivo*.

To overcome the limitations of conventional PDT, which is only applicable to superficial cancers, UCNP-based PDT, which can afford greater tissue penetration depths, can be employed. After effective RET, the surrounding PS can potentially exert its full therapeutic potential.[42,64] In addition, the multicolor-emission capability of NIR-excitable UCNPs allows for the simultaneous activation of dual PSs to enhance PDT. For example, UCNPs coated with a mesoporous silica shell layer were reported by Zhang *et al.* to deliver high payloads of two PSs, namely, merocyanine 540 (MC540) and zinc(II) phthalocyanine (ZnPc).[65] The surface modification of FA also accounts for the preferential accumulation of B16-F0 melanoma tumors *in vivo*. Irradiating these UCNPs with a 980-nm laser, resulting in UCL as green and red light (~540 and ~660 nm, respectively), can simultaneously activate the coloaded PS cargo, resulting in the enhanced generation of cytotoxic singlet oxygen. Compared with the single PS method, the dual-PS approach demonstrates greater PDT efficacy both *in vitro* and *in vivo*, achieving desirable therapeutic outcomes. In addition, because the absorption of water is stronger near 980 nm, the excitation of UCNPs should be performed at 700–850 nm to improve the tissue penetration depth and prevent overheating.[39] Various Nd^{3+}-sensitized UCNPs have been designed to provide laser excitation ability at 800 nm.[39,66] For example, Nd^{3+}-sensitized core–shell UCNPs have been used as dual-PS nanoplatforms for

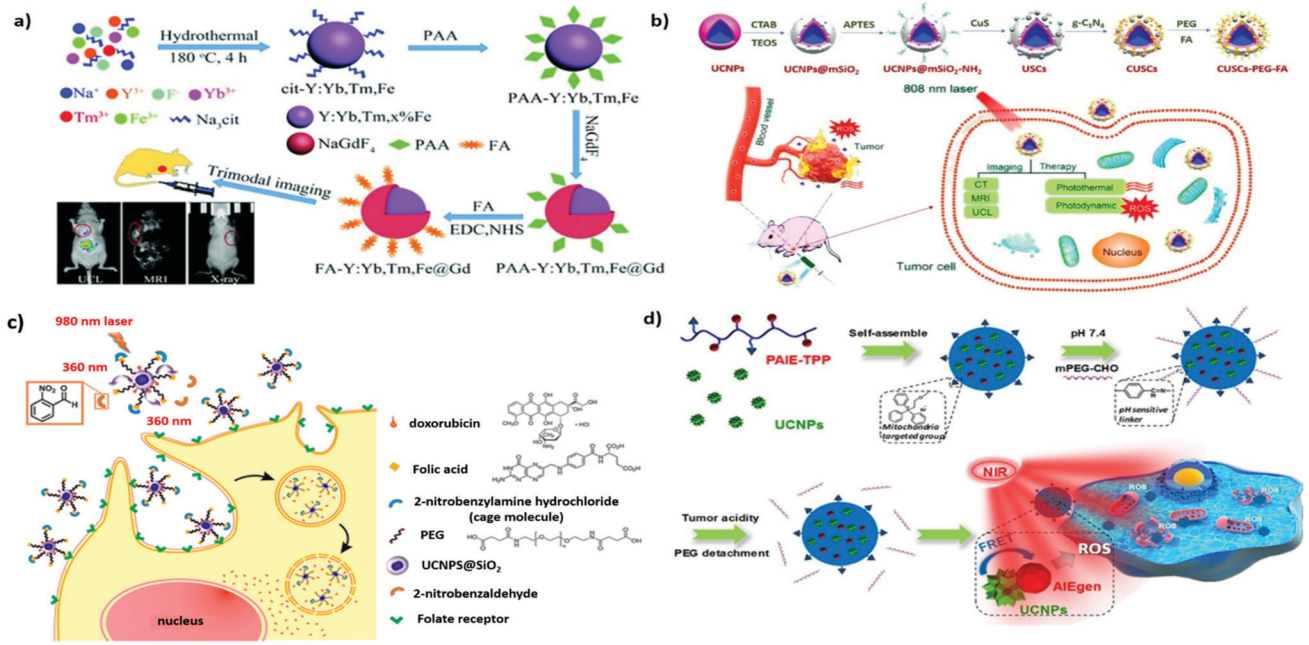

Fig. 3 FA- or TPP-functionalized UNCPs applied to active tumor targeting for drug delivery or biomedical imaging. (a) Preparation and surface modification of the FA-Y:Yb,Tm,Fe@Gd NPs for trimodal tumor imaging. Reproduced from ref. 63 with permission from The Royal Society of Chemistry. (b) Schematic illustration of the synthesis of the CUSCs-PEG-FA nanocomposite for multimodal imaging-guided PTT/PDT *in vitro* and *in vivo*. Reproduced from ref. 70 with permission from Elsevier. (c) Illustration of photocaged UCNPs following NIR laser activation to remove cage molecules and subsequent targeting of cancer cells. Reproduced from ref. 73 with permission from the American Chemical Society. (d) pH-Responsive UCNP@PAIE-TPP-PEG NPs as the NIR triggered mitochondria targeting PS to generate ROS for PDT. Reproduced from ref. 74 with permission from the American Chemical Society.

smart FR targeting to maximize the antitumor efficacy of PDT while minimizing damage to normal tissues.[67] This is promising for the future development of non-invasive treatment for deep-seated tumors.

PTT is another non-invasive phototherapy treatment. Unlike PDT, which relies on the light-induced cytotoxicity of PSs, PTT employs photoabsorption agents to efficiently convert energy from incident light to heat for tumor ablation. Yang *et al.* demonstrated a promising strategy for the targeted and imaging-guided chemo-PT treatment of cancer involving the combination of UCNPs and protein-capped gold nanodots (GNDs@BSA).[68] UCNPs play a principal role because of their excellent UCL, whereas GNDs@BSA offers excellent X-ray attenuation in CT imaging and PT conversion performance. Because the emission of UCNPs overlaps with the SPR band of GNDs@BSA, the RET effect can enhance PTT efficacy under NIR laser irradiation. The introduction of FA and chemotherapy drug doxorubicin (DOX) further suggests the improved anticancer efficiency of the combination of enhanced tumor accumulation and chemo-PT therapy. The combination of PTT and PDT can synergistically improve the efficiency of tumor treatment. An appropriate level of thermal effect can also increase the blood flow and thus the transport of oxygen to the tumor, leading to PT-enhanced PDT effects.[69] A highly efficient multifunctional anticancer nanocomposite device was attained by assembling a PT agent (CuS NPs) and a PDT agent (g-C_3N_4 quantum dots) on Tm^{3+}-doped UCNPs after mesoporous silica coating, followed by FA modification (Fig. 3b).[70] Under excitation with NIR light at 808 nm, PTT–PDT treatment inhibited cancer more effectively than any monotherapy. Codoping with Gd^{3+} and Yb^{3+} ions also makes the nanoplatform applicable in CT and MRI for contrast enhancement, and it can be used in conjunction with UCL imaging to yield high-resolution, three-dimensional structural details. Recently, Linde Type A (LTA) zeolite-derived UCNPs were loaded with protoporphyrin (PpIX), DOX, and FA. They have been developed for multimodal synergetic therapy involving US and NIR light, including chemotherapy, PTT, PDT, and sonodynamic therapy (SDT), used to treat melanoma.[71] Due to the deeper penetration of US, SDT–PDT could synergistically act on tumors, especially in deep tumors. PTT could also be simultaneously initiated by NIR through Er^{3+}/Yb^{3+}-codoped UCNPs to further enhance the effect of PDT.

Delivering chemotherapeutics to the site of action through controlled release can reduce the systemic side effects commonly associated with chemotherapy. Lu *et al.* designed polymer-caged UCNPs to achieve NIR-controlled drug release in anticancer therapy.[72] A folate-conjugated light-responsive spiropyran-containing copolymer (*i.e.*, PSMN-FA) was self-assembled on mesoporous silica-coated UCNPs with preloaded drugs. Under irradiation with NIR at 980 nm, the caged UCNPs codoped with Yb^{3+} and Tm^{3+} emitted UCL in the UV region, driving the spiropyran to switch from the closed-loop state to the zwitterionic open-loop state. This structural transformation made the amphiphilic copolymer more hydrophilic and detachable from the UCNPs, leading to the on-site release of active drugs for improved therapeutic efficacy. Moreover, caged FA-UCNPs were developed by Yeh *et al.* to realize NIR-controlled phototargeting for improved tumor selectivity (Fig. 3c).[73] When the UCNPs were under laser irradiation at 980 nm, the UCL emission at 360 nm uncaged the photolabile *o*-nitrobenzyl group, enabling FA to target FR and deliver UCNPs to lysosomes *via* FR-mediated endocytosis. To exert a chemotherapeutic effect, DOX was thiolated on the surface of the UCNPs to form a disulfide bond cleavable by intracellular lysosomal enzymes. These caged UNCPs can be used as a universal nanoplatform to achieve phototargeting with different types of tumor-homing ligands. For pH-responsive and imaging-guided drug delivery, hybrid nanocomposites consisting of magnetic UCNPs and nanoscale MOFs have been successfully fabricated through a simple one-step approach.[75] The magnetic Gd^{3+}-doped UCNP, serving as an MR/UCL imaging agent, is coupled with MIL-53(Fe) to achieve high drug loading and pH-responsive payload release. Decoration with FA revealed the enhanced uptake of B16–F10 melanoma cells.

Aside from FA, various small molecules such as monosaccharides (mannose, glucose, galactose, and their derivatives) and biotin also hold great potential for targeted delivery.[61,76] Several small molecules have also been used for tissue-specific targeting. For example, bisphosphonates that can bind specifically to hydroxyapatite were selected for UCNP functionalization to achieve bone-targeted multimodal (MR/PET) imaging.[77] In addition, UCNPs modified with glycyrrhetinic acid (GA) have been applied for *in vivo* hepatocellular carcinoma due to the identification of relatively abundant levels of GA receptors on the liver cell membrane.[78] Subcellular organelle-specific delivery of biologically active payloads has been considered a promising strategy for improving efficacy. Mitochondria and cell nuclei play vital roles in maintaining cell homeostasis and thus constitute targets in cancer therapy.[79] For example, Gao *et al.* reported the use of triphenylphosphine (TPP) as a mitochondria-targeting moiety for guiding polymer-encapsulated UCNPs to participate in the PDT-induced mitochondrial ROS collapse and cell apoptosis (Fig. 3d).[74] The coated polymer, featuring aggregation-induced emission (AIE) characteristics, is an effective PS that can be activated by the upconverted energy of Tm^{3+}-doped UCNPs under laser irradiation at 980 nm. The subcellular targeting ability allows for the specific delivery of therapeutics to intracellular sites, yielding improved PDT effects. Similar results were also observed by Wang *et al.* in their study, UCNPs were functionalized with a transactivating transcriptional activator for mitochondrial targeting, thereby achieving PDT potency maximization.[80] In short, the use of organelle-targeting ligands represents an innovative approach to modern therapy.

3.2 Aptamers

Aptamers are a class of small single-stranded oligonucleotides (usually comprising 20–80 nucleotide residues) that can fold into unique tertiary structures determined primarily by their sequences. Aptamers can also interact with their cognate targets with high affinity and specificity due to the combination of multiple intermolecular interactions; consequently, they are called ''chemical antibodies.'' In 1990, two research groups, Ellington and Szostak[81] and Tuerk and Gold,[82] described the process by which small nucleic acids (aptamers) specific to

targeted ligands are selected from synthetic combinatorial nucleic acid libraries through a technique called the systematic evolution of ligands by exponential enrichment (SELEX). Inspired by these breakthroughs, researchers have generated numerous DNA and RNA aptamers against various targets, ranging from small molecules to entire organisms.[83–85] Their low cost, small size, high thermal and chemical stability, ease of modification, and low immunogenicity make them promising alternatives to antibodies because they can be adapted to different applications.[83,86]

In 2006, Tan *et al.* proposed the first cell-based SELEX technique. In this process, a human acute lymphoblastic leukemia cell line, CCRF-CEM (T-cell line), was used as the target cell line, and a human diffuse large cell lymphoma cell line, Ramos (B-cell line), served as the control cell line.[87] Groups of aptamers have since been generated for the specific recognition of target cells. Among them, the DNA aptamer sgc8 has a strong affinity (K_d: ~0.8 nM) to the target protein tyrosine kinase 7 on the cell membrane,[87,88] which has recently been identified as a potential new biomarker for leukemia.[89] Tan *et al.* further designed a UNCP-based nanosystem for target cell–activatable fluorescence and MRI imaging.[90] MnO_2 nanolayers were grown *in situ* on the surfaces of UNCPs to quench the UCL. The sgc8 aptamer was surface conjugated to allow targeted delivery to CEM cells. After cellular uptake, the MnO_2 nanolayers were converted to Mn^{2+} through the reduction of intracellular glutathione, leading to the recovery of UCL and activatable MRI signals. The design of an "off–on" signal nanoprobe for tumor cell recognition provides new insights into the development of precision theranostics. Moreover, an sgc8c-based multifunctional DNA ligand was developed for UCNP surface modification (UCNP-Ce6-aptamer) to realize targeted PDT and bioimaging.[91] The DNA sequence was carefully designed to ensure the close proximity of Ce6 and UCNP to achieve effective RET and $^1O_2$ generation (Fig. 4a). The nanoplatform labeled with tetramethylrhodamine (TAMRA) dye at the end of the aptamer can also be used for biological imaging. Due to the high programmability of DNA, this approach can also be applied to deliver other therapeutic cargos in a NIR-responsive manner.

AS1411, a 26-mer guanidine-rich DNA aptamer discovered by Bates *et al.* that can bind to nucleolin with high affinity and specificity, exerts potent antiproliferative effects on various cancer cells but has little or no effect on nonmalignant cells.[92] AS1411 is in phase II clinical trials for the potential treatment of cancers including acute myeloid leukemia and renal cell carcinoma.[93] Studies have also demonstrated that AS1411 can function as a targeting agent for mediating cancer-selective drug delivery based on multiple nanoplatforms such as UCNP@MOF-DOX.[94] In addition, an AS1411-based smart DNA nanodevice was successfully constructed to recognize targets in tumors and generate photodynamic antitumor effects in a spatiotemporally controlled manner.[95] Specifically, the UCNP surface was coated with a mesoporous silica shell for the modification of UV light-activatable aptamer modules (L-Apt) and loaded with rose bengal (RB) (Fig. 4b). UCNPs can act as photoregulators to locally and orthogonally convert NIR light at 808 and 980 nm into UV and green UCL to sequentially activate programmed tumor recognition and PDT. This design allows tumor recognition and

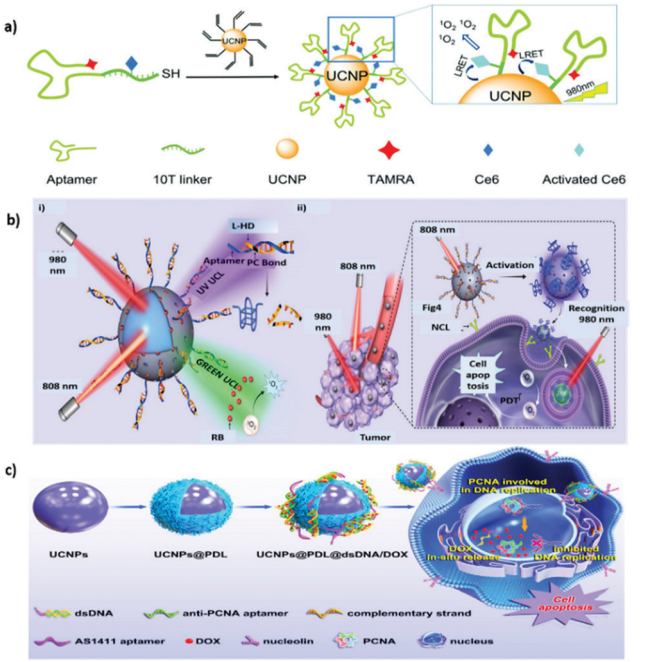

Fig. 4 Aptamer-functionalized UNCPs for active tumor targeting. (a) Schematic representation of the synthesis and $^1O_2$ generation mechanism of UCNP–Ce6–aptamer. Reproduced from ref. 91 with permission from The Royal Society of Chemistry. (b) Schematic showing (i) the orthogonal photoactivation of the DNA nanodevice in response to two NIR light of different wavelengths for (ii) programmed tumor recognition and PDT. Reproduced from ref. 95 with permission from the American Association for the Advancement of Science. (c) Procedure of the designed UCNPs@PDL@dsDNA/DOX nanotheranostic agent as the highly localized drug-delivery system. Reproduced from ref. 96 with permission from Frontiers.

PDT treatment with improved spatiotemporal precision. When combined with immune checkpoint blockade therapy, the nanodevice exerted both synergistic and abscopal effects in tumor-bearing mice. Furthermore, in consideration of the enhanced affinity and specificity associated with multivalency in natural systems, DNA nanotrains consisting of heterodimeric aptamers were developed for UCNP modification to achieve therapeutic benefits through effective nuclear localization.[96] A DNA sequence containing the AS1411 domain was hybridized with a partially complementary linker strand, which also contained the sequence of the antiproliferative cell nuclear antigen (PCNA) aptamer, to form a sequential duplex region rich in guanine and cytosine providing multiple loading sites for DOX (Fig. 4c). Driven by AS1411, the designed theranostic nanoplatform can be selectively endocytosed into cancer cells overexpressing nucleolin. The anti-PCNA aptamer is responsible for the nuclear translocation of therapeutic cargo. As expected, this nanoplatform produces superior pharmacological effects to DOX molecules alone, dramatically inhibiting the growth of tumors *in vivo*.

3.3 Proteins, antibodies, and peptides

Proteins, antibodies, antibody fragments, and peptides are of great interest as cancer-specific ligands due to their inherent high specificity toward their targets. Transferrin (Tf), a serum

glycoprotein responsible for iron transport in the body, is a widely studied targeting ligand. Upregulation of the transferrin receptor (TfR) ascribable to the elevated demand for iron has been reported in numerous cancers.[97,98] TfR-targeted transferrin or antibody fragments, such as single-chain variable fragments, have entered clinical trials for the development of various nanotherapeutics, including MBP-426, CALAA-01, SGT-53, and SGT-94, against different types of tumors.[99] The unique UCL characteristics of UCNPs can explain the achievement of NIR PDT *in vitro* by Tf-coated UNCPs.[100] When paramagnetic Gd^{3+} dopants were used, the resultant UCNP@Tf-PpIX also exhibited magnetically enhanced PDT efficiency in the presence of an external magnetic field. In addition, Tf can bind titanocene (Tc) at the iron-chelating epitope with an affinity equivalent to that of iron. Accordingly, Wu *et al.* designed a multilayered UCNP codoped with Yb^{3+} and Tm^{3+} featuring dual photosensitizing functions. A conjugated polymer is used as the first layer to generate $^1O_2$ through visible UCL, and apo-Tf-Tc is used as the second layer to generate peroxy radicals through UV UCL.[101] Using UCNP-based multimodal UCL, the dual ROS generation in response to NIR irradiation can induce formidable anticancer effects in deep tissues.

In addition to endogenous protein ligands, numerous antibodies have been developed to promote active targeting. The US Food and Drug Administration has approved more than 40 antibodies for cancer therapy, including those that can target receptors of interest such as the epidermal growth factor receptor or human epidermal growth factor receptor 2.[102] In addition, antibody conjugation with small, highly cytotoxic molecules called antibody–drug conjugates constitute a form of active targeted chemotherapy.[103] A similar approach has also been applied in targeted molecular imaging.[104] Bu *et al.* reported the use of carcinoembryonic antigen (CEA) antibody to modify the surface of Gd^{3+}-doped UCNP for targeted imaging of early colon cancer with CEA overexpression.[105] CEA-UCNPs are effective contrast agents that can contribute to the considerable enhancement of MR/UCL dual-mode imaging performance. Epithelial cell adhesion molecule (EpCAM; also known as CD326), a type I transmembrane glycoprotein that is overexpressed in epithelial cancers but is less highly expressed in normal epithelial tissues, is a favorable target for tumor therapy.[106,107] To mediate the immobilization of silica-coated UCNPs with anti-EpCAM antibodies in a specific orientation to improve accessibility, a bifunctional fusion protein, consisting of a silica-specific solid-binding peptide (referred to as the Linker, L) genetically fused to the N-terminus of Streptococcus Protein G′ (PG, an Ab-binding protein), was applied (Fig. 5a).[108] The resulting nanoplatform was confirmed to be useful for targeted UCL imaging and UCNP-based PDT for the selective eradication of cancer cells *in vitro*. EpCAM, which plays a key role in tumor progression, invasion, and metastasis, is also considered

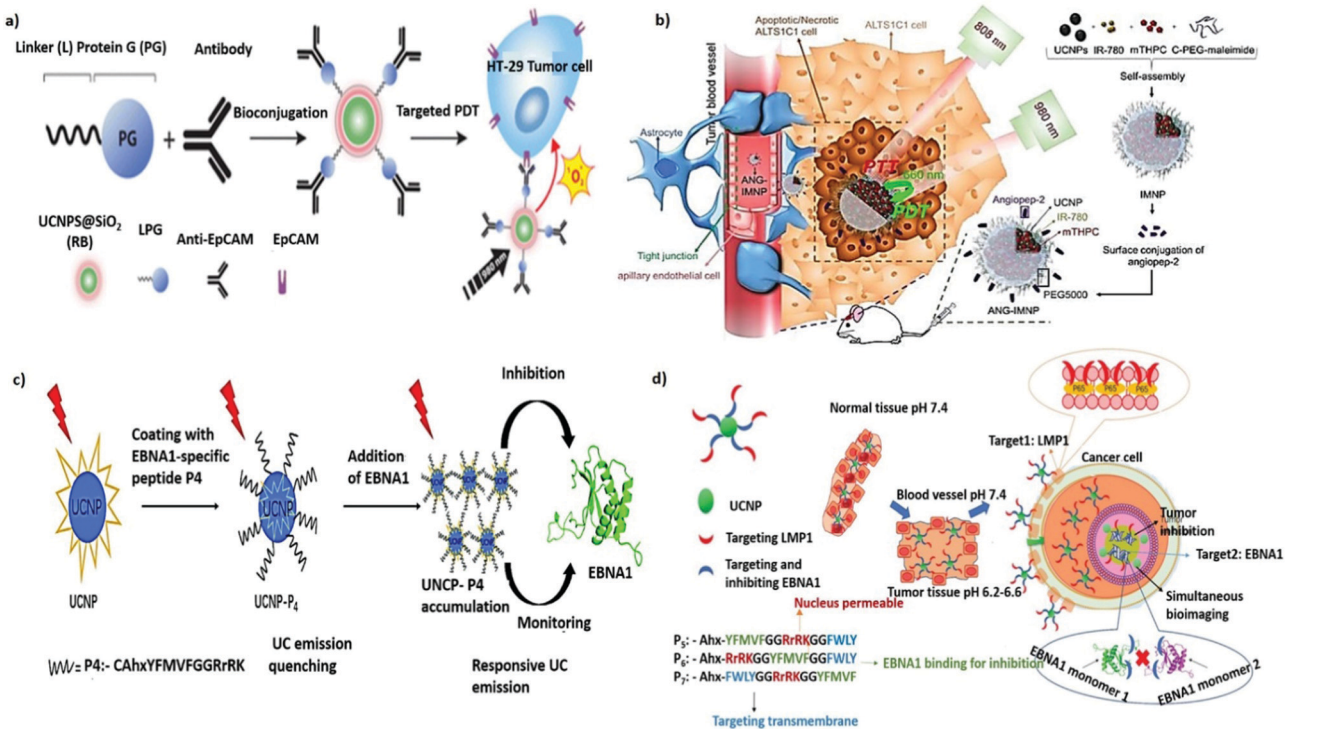

Fig. 5 Protein- or peptide-functionalized UNCPs for active tumor targeting. (a) Schematic illustration of LPG-mediated bioconjugation of UCNP@-SiO_2(RB) with antibodies and their application in targeted PDT. Reproduced from ref. 108 with permission from the American Chemical Society. (b) Illustration of active BBB penetration and the PT/PDT design of ANG-IMNPs in an orthotopic glioblastoma tumor model. Reproduced from ref. 122 with permission from Ivyspring International Publisher. (c) Schematic illustration of the dual-function for imaging and inhibition of UCNP-P4 in EBNA1 dimerization. Reproduced from ref. 124 with permission from The Royal Society of Chemistry. (d) Schematic illustration showing the path of entry of the nanoprobe UCNP-P_n, into an EBV-infected cancer cell from normal tissues through sequential and selective targeting. Reproduced from ref. 125 with permission from Wiley-VCH GmbH.

as a cancer stem cell biomarker.[109] Tang *et al.* reported on a simple strategy for surface engineering antihuman EpCAM on UCNP-based micelles to allow active targeted MR/UCL imaging in pancreatic cancer.[110] A similar strategy has also been applied for targeted mitoxantrone delivery in hepatocellular carcinoma to enable MRI/UCL-guided synergetic chemotherapy and PDT. Compared with a non-targeted counterpart, the combination with anti-EpCAM antibody can intensify its imaging contrast and antitumor action *in vivo*.[111]

Small peptides are gaining attention as targeting ligands for cancer therapy. Their advantages over antibodies include cost-effectiveness, ease of large-scale synthesis, high stability, and low immunogenicity.[112] The adhesion receptor integrin αvβ3, found to be overexpressed on tumor endothelial cells, can be specifically recognized by the cyclic and linear derivatives of the tripeptide arginine–glycine–aspartic acid (RGD).[113] Various RGD-conjugated UCNPs have also been exploited for the active targeting of different types of cancer cells *in vitro* and *in vivo*. For example, a high-contrast UCL label based on RGD-UCNPs was developed for the targeted imaging of tumors with deep tissue penetration (~600 μm).[114] In addition, a cyclic RGD-tethered amphiphilic polymer was used to coencapsulate UCNPs and photosensitizers with AIE characteristics. This novel theranostic nanoplatform exhibited great potential in the NIR PDT of deep-seated tumors with initial tumor volumes ranging from 60 to 240 mm^3.[115] Shen *et al.* also reported the use of NIR-to-red UCNPs to deliver Ce6-Mn complexes for T_1-weighted MRI and PDT. With acyclic RGD modification, the ability to target subcutaneous glioma tumors was greatly improved.[116] Moreover, cesium-doped UCNPs, which provide stronger X-ray attenuation, were also developed as an excellent CT/UCL contrast agent for RGD-mediated and imaging-guided chemo-PT cancer therapy.[117]

Integrins are known to play an essential role in tumor angiogenesis.[118] As such, the functionalization of UCNPs with ^{124}I-labeled RGD can be used as a multimodal PET/MRI/UCL nanoprobe for targeting tumor angiogenesis in cancer-specific diagnosis.[119] Similarly, UCNPs conjugated with Gd^{3+}-DOTA and RGD demonstrate preferential retention in subcutaneous U87MG tumor xenografts for successful MR/UCL imaging of glioblastoma.[120] However, due to the presence of the blood–brain barrier (BBB), drug delivery to brain tumors has always been a challenge. Angiopep-2 (ANG) is a promising glioma-targeting peptide that can interact with the low-density lipoprotein receptor-related protein-1 receptor on endothelial cells to mediate transcytosis and traverse the BBB.[121] As a result, ANG-conjugated UCNPs have great potential for enhanced accumulation in gliomas; as shown in Fig. 5b, they induced substantial cytotoxicity in an orthotopic model of NIR PDT and PTT against glioblastoma multiforme.[122] The KE108 peptide, a somatostatin analog possessing a strong binding affinity to somatostatin receptors, is commonly overexpressed in neuroendocrine (NE) tumors.[123] Aside from surgery, such tumors, including metastasized ones, can be effectively treated using KE108-functionalized UCNPs, which enable effective NE tumor targeting, as well as NIR PDT combined with chemotherapy with AB3.[126] Notably, a responsive UC nanoprobe was designed by Wang *et al.* to detect Epstein–Barr virus (EBV)-associated cancer.[124] Under the expression of the targeted protein Epstein–Barr nuclear antigen 1 (EBNA1), a latent cellular protein, in all EBV-associated tumor cells, UCNPs coated with an EBNA1-specific P4 peptide exhibited selective and responsive UC emission enhancement through aggregation (Fig. 5c). In 2021, the same group presented the next generation of bioprobes for the concurrent monitoring and inhibition of EBV-associated cancer cells (Fig. 5d).[125] Peptide sequences that can recognize two overexpressed EBV-specific oncoproteins, EBNA1 and the transmembrane protein LMP1, are introduced to UCNP surfaces through a pH-sensitive cleavable linker imine. Through the precise delivery guided by this dual-targeting peptide, the targeted UCNPs exhibit higher specific uptake, lesser side effects, and greater antitumor efficacy against EBV-positive tumors *in vivo*.

3.4 Hyaluronic acid (HA)

HA is an anionic, nonsulfated, naturally occurring glycosaminoglycan composed of repeating disaccharide units of β-1,4-D-glucuronic acid and β-1,3-D-*N*-acetylglucosamine. HA is abundant in the extracellular matrices of connective, epithelial, and neural tissues in vertebrates. The cell membrane interaction between HA and its receptor CD44 is pivotal to promoting tumor growth and metastasis.[127,128] Therefore, HA is considered as a promising ligand in the targeted delivery of various CD44-expressing tumor cells.[129,130] In 2017, Du *et al.* reported the use of HA-coated core–shell mesoporous UCNPs as a targeted drug delivery nanoplatform for the multimodal imaging-guided synergetic chemo-thermotherapy for breast cancer.[131] Contrary to the commonly used mesoporous silica shell, mesoporous $NaGdF_4$ is grown on the core of UCNPs to improve drug loading and imaging contrast. CuS acts as a gatekeeper to prevent premature drug leakage and improve PT and photoacoustic tomography (PAT) capabilities of the resulting nanocomposite. Surface grafting of HA also improves selective accumulation at the tumor site, and when used in combination with UCL/MR/PAT imaging, it can exert favorable theranostic effects. Another core–shell nanostructure (excited PS) and hypocrellin A (blue light-excited PS) were used to achieve HA-mediated dual-PS PDT through 808 nm light activation.[132] The TiO_2 shells can be crystallized directly on the surface of UCNPs for the stepwise conjugation of HA and hypocrellin A. Moreover, a layer-by-layer assembly approach was employed to generate multifunctional nanocomposites with UCNPs as the core and with Fe_3O_4 NPs and Prussian blue NPs (PBNPs) as the shell.[133] In the presence of HA and a magnetic field, a fourfold higher tumor accumulation rate (relative to that in the case without dual targeting) was obtained. PBNP decoration also allowed for sufficient PT ablation against targeted cancer cells under NIR irradiation. The resultant nanocomposites have great potential for application in MR/UCL/PAT imaging-guided, dual-targeted PTT *in vivo*. To realize controlled cargo release in a spatiotemporal manner, a sequentially responsive upconversion nano-onion (UCNO) with stacked polymer coating layers on UCNPs was designed by Ju *et al.* for small interfering RAN (siRNA) delivery.[134] The UCNPs were surface coated with RB-conjugated PEI (PEI-RB), ROS-responsive

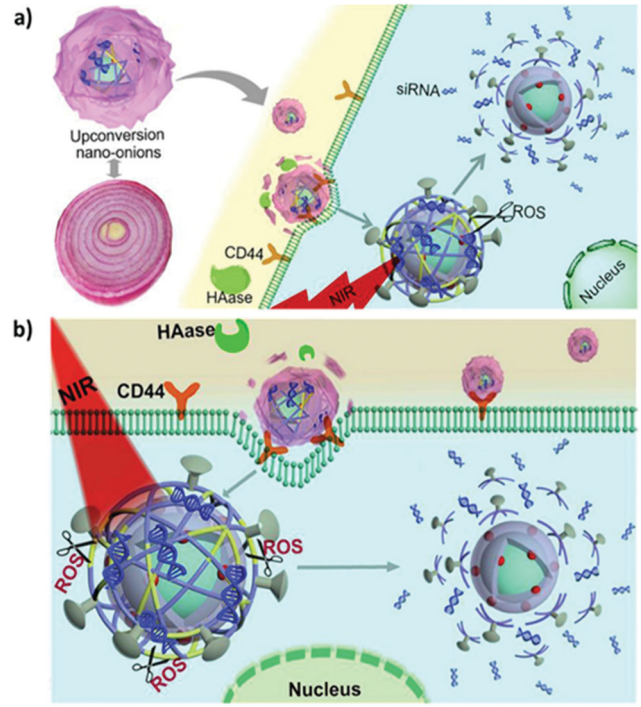

Fig. 6 HA-functionalised UCNPs for active tumor targeting. Schematic illustration of (a) synthesis of UCNOs (UCNP-PEIRB-PEISeSe/siRNA-R8-HA) and (b) sequential responsive decomposition of UCNOs and NIR boosted intracellular siRNA release and therapy. Reproduced from ref. 134 with permission from Elsevier.

diselenide-connected PEI (PEI-SeSe), siRNA, cell-penetrating peptide R8, and HA sequentially (Fig. 6a).

The negatively charged outer layer of HA both allows prolonged blood circulation and prevents nonspecific UCNO degradation. After efficient accumulation at the tumor site is achieved through HA-mediated active targeting, hyaluronidase can degrade the HA layer to expose the positively charged R8, leading to rapid cell internalization and lysosomal escape. UCL triggered by NIR light can activate PEI-RB to generate ROS and degrade the HA layer to expose the positively charged R8, leading to rapid cell internalization and lysosomal escape. UCL triggered by NIR light can activate PEI-RB to generate ROS and decompose the PEI-SeSe layer to release siRNA (Fig. 6b). The effectiveness of tumor growth suppression *in vivo* indicated the potential of the sequentially responsive UCNO in precision medicine.

3.5 Cell membrane camouflage

In targeted delivery, pegylation is the most commonly used method for improving the stealth properties of foreign NPs and nanovesicles. However, the interaction between the colloid surface and the plasma proteins (opsonins) is inevitable. This interaction promotes the rapid clearance of NPs from the bloodstream through the mononuclear phagocytic system, resulting in fast clearance and poor therapeutic efficacy.[135] Recently, various types of cell membranes such as those of red blood cells (RBCs), platelets, immune cells, and cancer cells have been explored to camouflage NPs in an attempt to determine the inherent properties and functions of the source cells.[136–139] After wrapping with cell membranes, biomimetic NPs exhibited high biocompatibility, immune evasion, long circulation time, and strong homotypic active targeting. This novel interfacing approach is believed to contribute to the development of future nanotechnology applications in medicine. For example, Liu *et al.* demonstrated that RBC membrane–coated UCNPs can minimize protein corona formation, thereby improving their FA-mediated tumor-targeting ability for enhanced UCL imaging *in vivo*.[140] In addition, a micro vehicle based on UCNP-decorated RBC was designed to achieve hypoxia-activated O_2 delivery and enhanced chemotherapy under NIR light.[141] The UNCP surfaces were functionalized with a hypoxia probe (HP) that can be transformed into an active state in a hypoxic microenvironment (Fig. 7a). Based on the RET process between UCNPs and active HP, the HP-emitted photoenergy can trigger the release of O_2 molecules from the oxy-hemoglobin carried in RBC under 980 nm light irradiation. On account of the tumor hypoxia alleviation, synchronous O_2

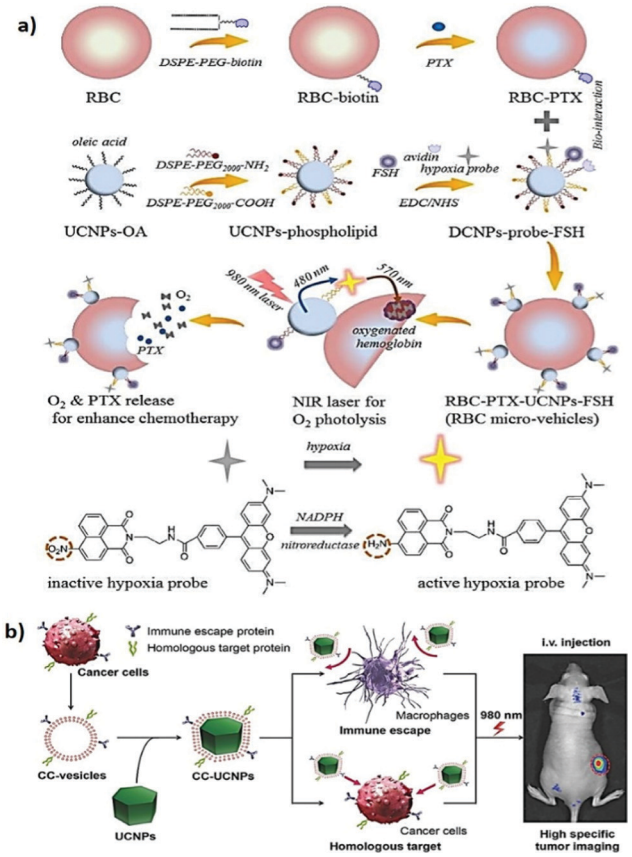

Fig. 7 Cell membrane camouflaged UCNPs for active tumor targeting. (a) Schematic illustration of RBCmv fabrication. In responsive to 980 nm laser irradiation, RBCmv can continuously release O_2 and PTX which endow the drug delivery system chemotherapy enhancement ability. Reproduced from ref. 141 with permission from The Royal Society of Chemistry. (b) Preparation, function, and application of CC-UCNPs. The resulting CC-UCNPs, which inherit the immune escaping and homologous targeting capabilities from the source cancer cells, have been used for highly specific tumor imaging. Reproduced from ref. 142 with permission from Wiley-VCH Verlag GmbH & Co. KGaA, Weinheim.

delivery can enhance the chemosensitivity of malignant tumor cells to conventional antitumor drugs (*e.g.*, paclitaxel, PTX). Moreover, cancer cell membrane–coated UCNPs (CC-UCNPs) were reported to evade immune clearance well, with an ability comparable to that of RBC-coated UCNPs.[142] CC-UCNPs also inherit source cancer cells' favorable homologous adhesion ability, enabling highly specific tumor targeting (Fig. 7b). Aside from the satisfactory NIR fluorescence emission performance of UCNPs, core–shell CC-UCNPs have been successfully used for highly specific *in vivo* tumor imaging.

In active targeting, recognition, retention and facilitated uptake of UCNPs can be enhanced by ligands that bind to specific receptors. In addition, surface grafting of multiple copies of ligand molecules on UCNPs can increase the overall avidity of NPs to the cognate target through cooperativity effects. The dual or multiple types of ligand molecules on a single nanoplatform also exhibited more effective cancer cell targeting than its corresponding single ligand system, collectively enhancing the binding efficiency and subsequent actions. However, there is no certitude of ''more-ligand-more-targeting''. A multitude of factors, such as ligand density, orientation and appropriate ligand combination, are critical aspects to achieve the desired outcomes of targeted delivery. Challenges including nonspecific plasma protein binding, low blood circulation rate, and poor biodistribution profile are also potential obstacles to be addressed for future cancer nanotheranostics.

4. Conclusion and future perspectives

This paper summarizes the recent advances in the design and use of UCNPs in tumor-targeted nanotherapeutics for cancer theranostics. We have provided accounts of various strategies for enhancing UCL efficiency and manipulating the multicolor emission and multimodal imaging capabilities of UCNPs. We have also introduced and discussed the latest progress in the surface engineering of UCNPs with the use of different types of bioligands for active tumor targeting. As has been demonstrated, the combination of targeting moieties with UCNP-based theranostic nanoplatforms has demonstrated substantial success with regard to applications in fields ranging from bioimaging to phototherapy. However, challenges in the implementation of UNCPs in precision medicine remain numerous.

First, consider renal excretion efficiency and toxicity. In general, NPs smaller than 10 nm in size can pass through the kidney after intravenous administration. Unfortunately, the luminescence efficiency of sub-10 nm UCNPs is usually dozens of times lower than that of UCNPs of typical sizes (50–60 nm). Therefore, the long-term cumulative toxicities and metabolic progress of targeted UCNPs (*e.g.*, through hepatobiliary excretion) require systematic investigation.

Second, the brightness of UCNPs requires improvement. Although UCL for bioimaging *in vivo* has been described under different circumstances, the low quantum yield (0.1–1%) remains a strict limitation even for UCNPs with designated core–shell architectures. Developing advanced strategies to enhance the brightness of core–shell UCNPs is essential, particularly for ultra-small (<10 nm) UCNPs.

Third, the tissue scattering effect remains an obstacle to visible UCL. NIR UCL represents a promising opportunity, but it is currently limited to Yb^{3+}/Tm^{3+} doping. Thus, the development of novel types of UCNPs allowing bright NIR-I (700–950 nm) or NIR-II (1000–1700 nm) downshifting luminescence is warranted. Because of the reduced scattering, minimal absorption, and negligible autofluorescence within these biological windows, centimeter-deep tissue imaging can be performed with high resolution and sensitivity.

Finally, UCNP-mediated PDT has been reported to activate the antitumor immune response by inducing immunogenic cell death and dendritic cell maturation. Alongside PDT, PTT, and NIR-responsive controlled drug release, targeted UCNPs also provide new means for photoimmunotherapy implementation, creating possibilities for the effective treatment of not only primary tumors but also metastatic or distant recurrent tumors.

Conflicts of interest

The authors declare no conflict of interest.

Acknowledgements

This work is supported by the Ministry of Science and Technology, Taiwan (MOST 108-2314-B-007-004-MY3, MOST 107-2221-E-007-032-MY3, MOST 109-2113-M-007-005, and 108-2638-M-002-001-MY2) and National Tsing Hua University, Taiwan (109Q2707E1). This manuscript was edited by Wallace Academic Editing.

References

1 K. Nurgali, R. T. Jagoe and R. Abalo, *Front. Pharmacol.*, 2018, **9**, 245.
2 X. Li, X.-N. Zhang, X.-D. Li and J. Chang, *Cancer Biol. Med.*, 2016, **13**, 339–348.
3 P. Padmanabhan, A. Kumar, S. Kumar, R. K. Chaudhary and B. Gulyás, *Acta Biomater.*, 2016, **41**, 1–16.
4 S. D. Jo, S. H. Ku, Y. Y. Won, S. H. Kim and I. C. Kwon, *Theranostics*, 2016, **6**, 1362–1377.
5 Y. Shi, R. van der Meel, X. Chen and T. Lammers, *Theranostics*, 2020, **10**, 7921–7924.
6 M. F. Attia, N. Anton, J. Wallyn, Z. Omran and T. F. Vandamme, *J. Pharm. Pharmacol.*, 2019, **71**, 1185–1198.
7 M. J. Mitchell, M. M. Billingsley, R. M. Haley, M. E. Wechsler, N. A. Peppas and R. Langer, *Nat. Rev. Drug Discovery*, 2021, **20**, 101–124.
8 N. Oh and J.-H. Park, *Int. J. Nanomed.*, 2014, **9**, 51–63.
9 J. Yoo, C. Park, G. Yi, D. Lee and H. Koo, *Cancers*, 2019, 11, 640.
10 S. Mura, J. Nicolas and P. Couvreur, *Nat. Mater.*, 2013, **12**, 991–1003.
11 Y. Qiao, J. Wan, L. Zhou, W. Ma, Y. Yang, W. Luo, Z. Yu and H. Wang, *Wiley Interdiscip. Rev.: Nanomed. Nanobiotechnol.*, 2019, **11**, e1527.

12 V. Estrella, T. Chen, M. Lloyd, J. Wojtkowiak, H. H. Cornnell, A. Ibrahim-Hashim, K. Bailey, Y. Balagurunathan, J. M. Rothberg, B. F. Sloane, J. Johnson, R. A. Gatenby and R. J. Gillies, *Cancer Res.*, 2013, **73**, 1524.
13 C. Wang, T. Zhao, Y. Li, G. Huang, M. A. White and J. Gao, *Adv. Drug Delivery Rev.*, 2017, **113**, 87–96.
14 J. Liu, Y. Huang, A. Kumar, A. Tan, S. Jin, A. Mozhi and X. J. Liang, *Biotechnol. Adv.*, 2014, **32**, 693–710.
15 V. Shanmugam, S. Selvakumar and C.-S. Yeh, *Chem. Soc. Rev.*, 2014, **43**, 6254–6287.
16 X. Ai, J. Mu and B. Xing, *Theranostics*, 2016, **6**, 2439–2457.
17 H. Zhu, P. Cheng, P. Chen and K. Pu, *Biomater. Sci.*, 2018, **6**, 746–765.
18 Z. Zhou, J. Song, L. Nie and X. Chen, *Chem. Soc. Rev.*, 2016, **45**, 6597–6626.
19 Y. Liu, P. Bhattarai, Z. Dai and X. Chen, *Chem. Soc. Rev.*, 2019, **48**, 2053–2108.
20 E. Hemmer, A. Benayas, F. Légaré and F. Vetrone, *Nanoscale Horiz.*, 2016, **1**, 168–184.
21 R. Vankayala and K. C. Hwang, *Adv. Mater.*, 2018, **30**, e1706320.
22 J. Zhao, D. Zhong and S. Zhou, *J. Mater. Chem. B*, 2018, **6**, 349–365.
23 S. Wu and H. J. Butt, *Adv. Mater.*, 2016, **28**, 1208–1226.
24 M. Haase and H. Schäfer, *Angew. Chem., Int. Ed.*, 2011, **50**, 5808–5829.
25 W. Zheng, P. Huang, D. Tu, E. Ma, H. Zhu and X. Chen, *Chem. Soc. Rev.*, 2015, **44**, 1379–1415.
26 A. Gnach, T. Lipinski, A. Bednarkiewicz, J. Rybka and J. A. Capobianco, *Chem. Soc. Rev.*, 2015, **44**, 1561–1584.
27 M. Sy, A. Nonat, N. Hildebrandt and L. J. Charbonnière, *Chem. Commun.*, 2016, **52**, 5080–5095.
28 G. Chen, H. Qiu, P. N. Prasad and X. Chen, *Chem. Rev.*, 2014, **114**, 5161–5214.
29 W. Fan, W. Bu and J. Shi, *Adv. Mater.*, 2016, **28**, 3987–4011.
30 B. Liu, C. Li, P. Yang, Z. Hou and J. Lin, *Adv. Mater.*, 2017, **29**, 1605434.
31 J. Xu, A. Gulzar, P. Yang, H. Bi, D. Yang, S. Gai, F. He, J. Lin, B. Xing and D. Jin, *Coord. Chem. Rev.*, 2019, **381**, 104–134.
32 X. Zhu, J. Zhang, J. Liu and Y. Zhang, *Adv. Sci.*, 2019, **6**, 1901358.
33 C. Chen, F. Wang, S. Wen, Q. P. Su, M. C. L. Wu, Y. Liu, B. Wang, D. Li, X. Shan, M. Kianinia, I. Aharonovich, M. Toth, S. P. Jackson, P. Xi and D. Jin, *Nat. Commun.*, 2018, **9**, 3290.
34 Q. Liu, Y. Sun, T. Yang, W. Feng, C. Li and F. Li, *J. Am. Chem. Soc.*, 2011, **133**, 17122–17125.
35 M. Bettinelli, L. Carlos and X. Liu, *Phys. Today*, 2015, **68**, 38–44.
36 J.-C. G. Bünzli and S. V. Eliseeva, *Chem. Sci.*, 2013, **4**, 1939–1949.
37 G. Jalani, V. Tam, F. Vetrone and M. Cerruti, *J. Am. Chem. Soc.*, 2018, **140**, 10923–10931.
38 F. Zhang, in *Photon Upconversion Nanomaterials*, ed. F. Zhang, Springer Berlin Heidelberg, Berlin, Heidelberg, 1st edn, 2015, ch. 1, pp. 1–20.
39 S. T. Dibaba, G. Xiaoqian, W. Ren and L. Sun, *J. Rare Earths*, 2019, **37**, 791–805.
40 N. Song, B. Zhou, L. Yan, J. Huang and Q. Zhang, *Front. Chem.*, 2019, **6**, 693.
41 L. M. Wiesholler, F. Frenzel, B. Grauel, C. Würth, U. Resch-Genger and T. Hirsch, *Nanoscale*, 2019, **11**, 13440–13449.
42 Y. Liu, X. Meng and W. Bu, *Coord. Chem. Rev.*, 2019, **379**, 82–98.
43 F. He, G. Yang, P. Yang, Y. Yu, R. Lv, C. Li, Y. Dai, S. Gai and J. Lin, *Adv. Funct. Mater.*, 2015, **25**, 3966–3976.
44 A. Bagheri, H. Arandiyan, C. Boyer and M. Lim, *Adv. Sci.*, 2016, **3**, 1500437.
45 E. Hong, L. Liu, L. Bai, C. Xia, L. Gao, L. Zhang and B. Wang, *Mater. Sci. Eng., C*, 2019, **105**, 110097.
46 F. Wang and X. Liu, *J. Am. Chem. Soc.*, 2008, **130**, 5642–5643.
47 V. Muhr, S. Wilhelm, T. Hirsch and O. S. Wolfbeis, *Acc. Chem. Res.*, 2014, **47**, 3481–3493.
48 F. Wang, C. Zhang, Q. Xue, H. Li and Y. Xian, *Biosens. Bioelectron.*, 2017, **95**, 21–26.
49 S. Wen, J. Zhou, P. J. Schuck, Y. D. Suh, T. W. Schmidt and D. Jin, *Nat. Photonics*, 2019, **13**, 828–838.
50 X. Wu, Y. Zhang, K. Takle, O. Bilsel, Z. Li, H. Lee, Z. Zhang, D. Li, W. Fan, C. Duan, E. M. Chan, C. Lois, Y. Xiang and G. Han, *ACS Nano*, 2016, **10**, 1060–1066.
51 J. Liu, F. Yang, M. Feng, Y. Wang, X. Peng and R. Lv, *ACS Biomater. Sci. Eng.*, 2019, **5**, 5051–5059.
52 D. Mendez-Gonzalez, S. Melle, O. G. Calderón, M. Laurenti, E. Cabrera-Granado, A. Egatz-Gómez, E. López-Cabarcos, J. Rubio-Retama and E. Díaz, *Nanoscale*, 2019, **11**, 13832–13844.
53 Y. Fan, L. Liu and F. Zhang, *Nano Today*, 2019, **25**, 68–84.
54 J.-N. Liu, W.-B. Bu and J.-L. Shi, *Acc. Chem. Res.*, 2015, **48**, 1797–1805.
55 Y. Zhang, X. Zhu and Y. Zhang, *ACS Nano*, 2021, **15**, 3709–3735.
56 W. Cai, J. Wang, C. Chu, W. Chen, C. Wu and G. Liu, *Adv. Sci.*, 2018, **6**, 1801526.
57 U. Kostiv, Z. Farka, M. J. Mickert, H. H. Gorris, N. Velychkivska, O. Pop-Georgievski, M. Pastucha, E. Odstrčilíková, P. Skládal and D. Horák, *Biomacromolecules*, 2020, **21**, 4502–4513.
58 A. Sedlmeier and H. H. Gorris, *Chem. Soc. Rev.*, 2015, **44**, 1526–1560.
59 C. Chen, J. Ke, X. E. Zhou, W. Yi, J. S. Brunzelle, J. Li, E. L. Yong, H. E. Xu and K. Melcher, *Nature*, 2013, **500**, 486–489.
60 M. Fernández, F. Javaid and V. Chudasama, *Chem. Sci.*, 2018, **9**, 790–810.
61 A. Sosnik, in *Biomedical Applications of Functionalized Nanomaterials*, ed. B. Sarmento and J. das Neves, Elsevier, Amsterdam, Netherlands, 1st edn, 2018, ch. 1, pp. 1–32.
62 L. Sun, Z. Wei, H. Chen, J. Liu, J. Guo, M. Cao, T. Wen and L. Shi, *Nanoscale*, 2014, **6**, 8878–8883.
63 Z. An, L. Wang, C. Gao, N. He, B. Zhu, Y. Liu and Q. Cai, *New J. Chem.*, 2018, **42**, 17073–17082.
64 H. Qiu, M. Tan, T. Y. Ohulchanskyy, J. F. Lovell and G. Chen, *Nanomaterials*, 2018, **8**, 344.

65 N. M. Idris, M. K. Gnanasammandhan, J. Zhang, P. C. Ho, R. Mahendran and Y. Zhang, *Nat. Med.*, 2012, **18**, 1580–1585.
66 D. Wang, B. Xue, X. Kong, L. Tu, X. Liu, Y. Zhang, Y. Chang, Y. Luo, H. Zhao and H. Zhang, *Nanoscale*, 2015, **7**, 190–197.
67 M. Yang, H. Wang, Z. Wang, Z. Han and Y. Gu, *Biomater. Sci.*, 2019, **7**, 1686–1695.
68 C. Wang, R. Xue, A. Gulzar, Y. Kuang, H. Shao, S. Gai, D. Yang, F. He and P. Yang, *Chem. Eng. J.*, 2019, **370**, 1239–1250.
69 Z. Shen, Q. Ma, X. Zhou, G. Zhang, G. Hao, Y. Sun and J. Cao, *NPG Asia Mater.*, 2021, **13**, 39.
70 M. Xu, G. Yang, H. Bi, J. Xu, L. Feng, D. Yang, Q. Sun, S. Gai, F. He, Y. Dai, C. Zhong and P. Yang, *Chem. Eng. J.*, 2019, **360**, 866–878.
71 L. Zheng, Y. Zhang, H. Lin, S. Kang, Y. Li, D. Sun, M. Chen, Z. Wang, Z. Jiao, Y. Wang, B. Dai, S. Zhuang and D. Zhang, *ACS Appl. Mater. Interfaces*, 2020, **12**, 32420–32431.
72 Q. Xing, N. Li, Y. Jiao, D. Chen, J. Xu, Q. Xu and J. Lu, *RSC Adv.*, 2015, **5**, 5269–5276.
73 Y.-H. Chien, Y.-L. Chou, S.-W. Wang, S.-T. Hung, M.-C. Liau, Y.-J. Chao, C.-H. Su and C.-S. Yeh, *ACS Nano*, 2013, **7**, 8516–8528.
74 Y. Guan, H. Lu, W. Li, Y. Zheng, Z. Jiang, J. Zou and H. Gao, *ACS Appl. Mater. Interfaces*, 2017, **9**, 26731–26739.
75 P. Mukherjee, A. Kumar, K. Bhamidipati, N. Puvvada and S. K. Sahu, *ACS Appl. Bio Mater.*, 2020, **3**, 869–880.
76 Z. Zhao, A. Ukidve, J. Kim and S. Mitragotri, *Cell*, 2020, **181**, 151–167.
77 S. Alonso-de Castro, E. Ruggiero, A. Lekuona Fernández, U. Cossío, Z. Baz, D. Otaegui, V. Gómez-Vallejo, D. Padro, J. Llop and L. Salassa, *Inorganics*, 2019, **7**, 60.
78 J. E. Choi, H.-K. Kim, Y. Kim, G. Kim, T. S. Lee, S. Kim, D. Kim and H. S. Jang, *Mater. Des.*, 2020, **195**, 108941.
79 A. Parodi, C. Corbo, A. Cevenini, R. Molinaro, R. Palomba, L. Pandolfi, M. Agostini, F. Salvatore and E. Tasciotti, *Nanomedicine*, 2015, **10**, 1923–1940.
80 X. Zhang, F. Ai, T. Sun, F. Wang and G. Zhu, *Inorg. Chem.*, 2016, **55**, 3872–3880.
81 A. D. Ellington and J. W. Szostak, *Nature*, 1990, **346**, 818–822.
82 C. Tuerk and L. Gold, *Science*, 1990, **249**, 505–510.
83 W. Tan, M. J. Donovan and J. Jiang, *Chem. Rev.*, 2013, **113**, 2842–2862.
84 Z. Zhuo, Y. Yu, M. Wang, J. Li, Z. Zhang, J. Liu, X. Wu, A. Lu, G. Zhang and B. Zhang, *Int. J. Mol. Sci.*, 2017, **18**, 2142.
85 P. Bayat, R. Nosrati, M. Alibolandi, H. Rafatpanah, K. Abnous, M. Khedri and M. Ramezani, *Biochimie*, 2018, **154**, 132–155.
86 J. Zhou and J. Rossi, *Nat. Rev. Drug Discovery*, 2017, **16**, 181–202.
87 D. Shangguan, Y. Li, Z. Tang, Z. C. Cao, H. W. Chen, P. Mallikaratchy, K. Sefah, C. J. Yang and W. Tan, *Proc. Natl. Acad. Sci. U. S. A.*, 2006, **103**, 11838–11843.
88 D. Shangguan, Z. Cao, L. Meng, P. Mallikaratchy, K. Sefah, H. Wang, Y. Li and W. Tan, *J. Proteome Res.*, 2008, **7**, 2133–2139.
89 G. Jiang, M. Zhang, B. Yue, M. Yang, C. Carter, S. Z. Al-Quran, B. Li and Y. Li, *Leuk. Res.*, 2012, **36**, 1347–1353.
90 Y. Wu, D. Li, F. Zhou, H. Liang, Y. Liu, W. Hou, Q. Yuan, X. Zhang and W. Tan, *Chem. Sci.*, 2018, **9**, 5427–5434.
91 W. Hou, Y. Liu, Y. Jiang, Y. Wu, C. Cui, Y. Wang, L. Zhang, I. T. Teng and W. Tan, *Nanoscale*, 2018, **10**, 10986–10990.
92 P. J. Bates, D. A. Laber, D. M. Miller, S. D. Thomas and J. O. Trent, *Exp. Mol. Pathol.*, 2009, **86**, 151–164.
93 J. E. Rosenberg, R. M. Bambury, E. M. Van Allen, H. A. Drabkin, P. N. Lara, Jr., A. L. Harzstark, N. Wagle, R. A. Figlin, G. W. Smith, L. A. Garraway, T. Choueiri, F. Erlandsson and D. A. Laber, *Invest. New Drugs*, 2014, **32**, 178–187.
94 K. Deng, Z. Hou, X. Li, C. Li, Y. Zhang, X. Deng, Z. Cheng and J. Lin, *Sci. Rep.*, 2015, **5**, 7851.
95 Z. Di, B. Liu, J. Zhao, Z. Gu, Y. Zhao and L. Li, *Sci. Adv.*, 2020, **6**, eaba9381.
96 X. Song, T. Yan, F. Tian, F. Li, L. Ren, Q. Li and S. Zhang, *Front. Bioeng. Biotechnol.*, 2021, **9**, 639487.
97 Y. Shen, X. Li, D. Dong, B. Zhang, Y. Xue and P. Shang, *Am. J. Cancer Res.*, 2018, **8**, 916–931.
98 T. R. Daniels, E. Bernabeu, J. A. Rodríguez, S. Patel, M. Kozman, D. A. Chiappetta, E. Holler, J. Y. Ljubimova, G. Helguera and M. L. Penichet, *Biochim. Biophys. Acta*, 2012, **1820**, 291–317.
99 A. K. Pearce and R. K. O'Reilly, *Bioconjugate Chem.*, 2019, **30**, 2300–2311.
100 D. Wang, L. Zhu, Y. Pu, J.-X. Wang, J.-F. Chen and L. Dai, *Nanoscale*, 2017, **9**, 11214–11221.
101 S. Liu, Y. Yuan, Y. Yang, Z. Liu, S. Yin, W. Qin and C. Wu, *J. Mater. Chem. B*, 2017, **5**, 8169–8177.
102 A. Mullard, *Nat. Rev. Drug Discovery*, 2021, **20**, 491–495.
103 A. Beck, L. Goetsch, C. Dumontet and N. Corvaïa, *Nat. Rev. Drug Discovery*, 2017, **16**, 315–337.
104 J. M. Warram, E. de Boer, A. G. Sorace, T. K. Chung, H. Kim, R. G. Pleijhuis, G. M. van Dam and E. L. Rosenthal, *Cancer Metastasis Rev.*, 2014, **33**, 809–822.
105 Y. Jin, D. Ni, J. Zhang, F. Han, J. Wang, L. Gao, H. Zhang, Y. Liu, Z. Cui, Z. Yao, X. Feng and W. Bu, *Part. Part. Syst. Charact.*, 2017, **34**, 1600393.
106 M. Trzpis, P. M. McLaughlin, L. M. de Leij and M. C. Harmsen, *Am. J. Pathol.*, 2007, **171**, 386–395.
107 S. Imrich, M. Hachmeister and O. Gires, *Cell Adhes. Migr.*, 2012, **6**, 30–38.
108 L. Liang, A. Care, R. Zhang, Y. Lu, N. H. Packer, A. Sunna, Y. Qian and A. V. Zvyagin, *ACS Appl. Mater. Interfaces*, 2016, **8**, 11945–11953.
109 M. A. Mohtar, S. E. Syafruddin, S. N. Nasir and T. Y. Low, *Biomolecules*, 2020, **10**, 255.
110 Y. Han, Y. An, G. Jia, X. Wang, C. He, Y. Ding and Q. Tang, *J. Nanobiotechnol.*, 2018, **16**, 7.
111 Y. Han, Y. An, G. Jia, X. Wang, C. He, Y. Ding and Q. Tang, *Nanoscale*, 2018, **10**, 6511–6523.
112 E. Ruoslahti, *Adv. Mater.*, 2012, **24**, 3747–3756.
113 S. Liu, *Bioconjugate Chem.*, 2009, **20**, 2199–2213.
114 L. Xiong, Z. Chen, Q. Tian, T. Cao, C. Xu and F. Li, *Anal. Chem.*, 2009, **81**, 8687–8694.
115 G. Jin, R. He, Q. Liu, M. Lin, Y. Dong, K. Li, B. Z. Tang, B. Liu and F. Xu, *Theranostics*, 2019, **9**, 246–264.

116 X. L. Tang, J. Wu, B. L. Lin, S. Cui, H. M. Liu, R. T. Yu, X. D. Shen, T. W. Wang and W. Xia, *Acta Biomater.*, 2018, **74**, 360–373.
117 Y. Liu, L. Li, Q. Guo, L. Wang, D. Liu, Z. Wei and J. Zhou, *Theranostics*, 2016, **6**, 1491–1505.
118 B. Garmy-Susini and J. A. Varner, *Lymphatic Res. Biol.*, 2008, **6**, 155–163.
119 J. Lee, T. S. Lee, J. Ryu, S. Hong, M. Kang, K. Im, J. H. Kang, S. M. Lim, S. Park and R. Song, *J. Nucl. Med.*, 2013, **54**, 96–103.
120 J. Jin, Z. Xu, Y. Zhang, Y. J. Gu, M. H. Lam and W. T. Wong, *Adv. Healthcare Mater.*, 2013, **2**, 1501–1512.
121 X. Zhou, Q. R. Smith and X. Liu, *Wiley Interdiscip. Rev.: Nanomed. Nanobiotechnol.*, 2021, **13**, e1695.
122 Y.-C. Tsai, P. Vijayaraghavan, W.-H. Chiang, H.-H. Chen, T.-I. Liu, M.-Y. Shen, A. Omoto, M. Kamimura, K. Soga and H.-C. Chiu, *Theranostics*, 2018, **8**, 1435–1448.
123 G. Chen, R. Jaskula-Sztul, A. Harrison, A. Dammalapati, W. Xu, Y. Cheng, H. Chen and S. Gong, *Biomaterials*, 2016, **97**, 22–33.
124 S. Zha, Y. H. Fung, H. F. Chau, P. Ma, J. Lin, J. Wang, L. S. Chan, G. Zhu, H. L. Lung and K. L. Wong, *Nanoscale*, 2018, **10**, 15632–15640.
125 S. Zha, H.-F. Chau, W. Y. Chau, L. S. Chan, J. Lin, K. W. Lo, W. C.-S. Cho, Y. L. Yip, S. W. Tsao, P. J. Farrell, L. Feng, J. M. Di, G.-L. Law, H. L. Lung and K.-L. Wong, *Adv. Sci.*, 2021, **8**, 2002919.
126 G. Chen, R. Jaskula-Sztul, C. R. Esquibel, I. Lou, Q. Zheng, A. Dammalapati, A. Harrison, K. W. Eliceiri, W. Tang, H. Chen and S. Gong, *Adv. Funct. Mater.*, 2017, **27**, 1604671.
127 B. P. Toole, *Clin. Cancer Res.*, 2009, **15**, 7462–7468.
128 S. Misra, V. C. Hascall, R. R. Markwald and S. Ghatak, *Front. Immunol.*, 2015, **6**, 201.
129 Z. Luo, Y. Dai and H. Gao, *Acta Pharm. Sin. B*, 2019, **9**, 1099–1112.
130 J. Huang, L. Zhang, D. Wan, L. Zhou, S. Zheng, S. Lin and Y. Qiao, *Signal Transduction Targeted Ther.*, 2021, **6**, 153.
131 X. Su, F. Zhao, Y. Wang, X. Yan, S. Jia and B. Du, *Nanomedicine*, 2017, **13**, 1761–1772.
132 Z. Hou, K. Deng, C. Li, X. Deng, H. Lian, Z. Cheng, D. Jin and J. Lin, *Biomaterials*, 2016, **101**, 32–46.
133 B. Du, X. Cao, F. Zhao, X. Su, Y. Wang, X. Yan, S. Jia, J. Zhou and H. Yao, *J. Mater. Chem. B*, 2016, **4**, 2038–2050.
134 Y. He, S. Guo, L. Wu, P. Chen, L. Wang, Y. Liu and H. Ju, *Biomaterials*, 2019, **225**, 119501.
135 H. H. Gustafson, D. Holt-Casper, D. W. Grainger and H. Ghandehari, *Nano Today*, 2015, **10**, 487–510.
136 Z. Amoozgar and Y. Yeo, *Wiley Interdiscip. Rev.: Nanomed. Nanobiotechnol.*, 2012, **4**, 219–233.
137 R. Li, Y. He, S. Zhang, J. Qin and J. Wang, *Acta Pharm. Sin. B*, 2018, **8**, 14–22.
138 Q. Xia, Y. Zhang, Z. Li, X. Hou and N. Feng, *Acta Pharm. Sin. B*, 2019, **9**, 675–689.
139 B. Choi, W. Park, S.-B. Park, W.-K. Rhim and D. K. Han, *Methods*, 2020, **177**, 2–14.
140 L. Rao, Q.-F. Meng, L.-L. Bu, B. Cai, Q. Huang, Z.-J. Sun, W.-F. Zhang, A. Li, S.-S. Guo, W. Liu, T.-H. Wang and X.-Z. Zhao, *ACS Appl. Mater. Interfaces*, 2017, **9**, 2159–2168.
141 P. Wang, S. Jiang, Y. Li, Q. Luo, J. Lin, L. Hu, C. Xu, J. Zhu and L. Fan, *Biomater. Sci.*, 2020, **8**, 4595–4602.
142 L. Rao, L.-L. Bu, B. Cai, J.-H. Xu, A. Li, W.-F. Zhang, Z.-J. Sun, S.-S. Guo, W. Liu, T.-H. Wang and X.-Z. Zhao, *Adv. Mater.*, 2016, **28**, 3460–3466.